

MICROCOPY RESOLUTION TEST CHART  
NATIONAL BUREAU OF STANDARDS-1963-A

2

# NAVAL POSTGRADUATE SCHOOL Monterey, California

AD-A161 057



DTIC  
ELECTE  
NOV 12 1985  
S E D

## THESIS

AN INVESTIGATION OF THE ATMOSPHERIC BOUNDARY LAYER  
OVER THE ARCTIC OCEAN USING SODAR

by

Etienne de Rougé

September 1985

Thesis Advisor:

W. J. Shaw

DTIC FILE COPY

Approved for public release; distribution is unlimited.

85 11 12 08 5

REPORT DOCUMENTATION PAGE		READ INSTRUCTIONS BEFORE COMPLETING FORM
1. REPORT NUMBER	2. GOVT ACCESSION NO. AD-A161057	3. RECIPIENT'S CATALOG NUMBER
4. TITLE (and Subtitle) An Investigation of the Atmospheric Boundary Layer over the Arctic Ocean Using SODAR		5. TYPE OF REPORT & PERIOD COVERED Master's Thesis; September 1985
7. AUTHOR(s)  Etienne de Rougé		6. PERFORMING ORG. REPORT NUMBER
9. PERFORMING ORGANIZATION NAME AND ADDRESS Naval Postgraduate School Monterey, California 93943		8. CONTRACT OR GRANT NUMBER(s)
11. CONTROLLING OFFICE NAME AND ADDRESS Naval Postgraduate School Monterey, California 93943		10. PROGRAM ELEMENT, PROJECT, TASK AREA & WORK UNIT NUMBERS
14. MONITORING AGENCY NAME & ADDRESS (if different from Controlling Office)		12. REPORT DATE September 1985
		13. NUMBER OF PAGES 79
		15. SECURITY CLASS. (of this report)
		15a. DECLASSIFICATION/DOWNGRADING SCHEDULE
16. DISTRIBUTION STATEMENT (of this Report)  Approved for public release; distribution is unlimited.		
17. DISTRIBUTION STATEMENT (of the abstract entered in Block 20, if different from Report)		
18. SUPPLEMENTARY NOTES		
19. KEY WORDS (Continue on reverse side if necessary and identify by block number) Sodar Atmospheric Boundary Layer Refractivity <i>(Unusual Terms)</i>		
20. ABSTRACT (Continue on reverse side if necessary and identify by block number) An attempt to describe the atmospheric boundary layer during the MIZEX 84 from 11 July to 17 July was made using a sodar system. The computation of the temperature structure parameter $CT^2$ in the surface layer using <u>in situ</u> measurements allowed the calibration of the system. $CT^2$ was found to have the following functional dependence on the backscattered signal I:		

$$\text{Log}(CT^2) = 8.63\text{Log}(I) - 25.66.$$

Time-height cross-sections showed very well the structure of the boundary layer. An especially good representation of the strength of  $CT^2$  in the inversion layer was achieved.

→ A program was developed to obtain the inversion layer height  $Z_i$ , where the signal reaches a maximum. The thickness of the inversion layer was also computed and was used with the calibration law to compute  $CT^2$  at the inversion layer. This allowed the computation of the jump of potential temperature and the refractive index gradient in the inversion under free convection. → Refractive trapping conditions were evident on 15 July although the generally small value of the heat flux did not indicate a strongly unstable boundary layer. Comparison with two radiosonde profiles shows good agreement in one case, but does not permit a reliable conclusion to be made concerning the method. However, the procedure could be extended to other areas, especially those with strong free convection. The method should provide a good estimate of the refractive condition in the atmospheric boundary layer.

Approved for public release; distribution is unlimited.

*An Investigation of the Atmospheric Boundary Layer  
over the Arctic Ocean using Sodar*

by

Etienne de Rouge  
Lieutenant de Vaisseau, French Navy

Submitted in partial fulfillment of the  
requirements for the degree of

MASTER OF SCIENCE IN OCEANOGRAPHY

from the

NAVAL POSTGRADUATE SCHOOL  
September 1985

Accession For	
NTIS GRA&I	<input checked="" type="checkbox"/>
DTIC TAB	<input type="checkbox"/>
Unannounced	<input type="checkbox"/>
Justification	
By _____	
Distribution/	
Availability Codes	
Dist	Avail and/or Special
A-1	

Author:

*Etienne de Rouge*  
Etienne de Rouge

Approved by:

*W.J. Shaw*  
W.J. Shaw, Thesis Advisor

*Roland W. Garwood*  
R.W. Garwood, Second Reader

*C.N.K. Mooers*  
C.N.K. Mooers, Chairman,  
Department of Oceanography

*John N. Dyer*  
John N. Dyer,  
Dean of Science and Engineering

REPRODUCED AT GOVERNMENT EXPENSE



## ABSTRACT

An attempt to describe the atmospheric boundary layer during the MIZEX 84 from 11 July to 17 July was made using a sodar system. The computation of the temperature structure parameter  $CT^2$  in the surface layer using *in situ* measurements allowed the calibration of the system.  $CT^2$  was found to have the following functional dependence on the backscattered signal I:

$$\text{Log}(CT^2) = 8.63\text{Log}(I) - 25.66.$$

Time-height cross-sections showed very well the structure of the boundary layer. An especially good representation of the strength of  $CT^2$  in the inversion layer was achieved.

A program was developed to obtain the inversion layer height  $Z_i$ , where the signal reaches a maximum. The thickness of the inversion layer was also computed and was used with the calibration law to compute  $CT^2$  at the inversion layer. This allowed the computation of the jump of potential temperature and the refractive index gradient in the inversion under free convection. Refractive trapping conditions were evident on 15 July although the generally small value of the heat flux did not indicate a strongly unstable boundary layer. Comparison with two radiosonde profiles shows good agreement in one case, but does not permit a reliable conclusion to be made concerning the method. However, the procedure could be extended to other areas, especially those with strong free convection. The method should provide a good estimate of the refractive condition in the atmospheric boundary layer.

## RESUME

Un système sodar (Sound Detection and Ranging) a permis de recueillir des données concernant la couche limite atmosphérique entre le 11 et 17 juillet pendant l'opération MIZEX 1984. Le calcul du paramètre de structure de la température  $CT^2$  dans la couche de surface utilisant des mesures *in situ*, permet la calibration du système. Il apparait que  $CT^2$  est fonction du signal de réverbération direct  $I$  suivant la loi:

$$\log(CT^2) = \log(I) - 25.66.$$

Plusieurs coupe représentant  $CT^2$  en fonction du temps et de l'altitude montrent la structure de la couche limite et donnent une bonne représentation de la valeur de  $CT^2$  dans la couche d'inversion.

Un programme a été développé pour obtenir la hauteur de cette couche ou un signal maximum est atteint. L'épaisseur de cette couche est aussi calculée afin d'être utilisée avec la loi de calibration pour en déduire  $CT^2$  à chaque niveau. Ceci permet de trouver le saut de température potentielle et le gradient d'index de réfraction dans l'inversion en cas de convection libre. Pendant la journée du 15 juillet on remarque que les ondes électromagnétiques ont pu être "capturées" par la couche d'inversion, bien que la faible valeur du flux de chaleur n'ait pas été toujours conforme aux conditions d'instabilité requises. La comparaison avec quelques profils de radiosonde est bonne dans un cas, mais ne permet pas d'obtenir une conclusion certaine sur la méthode. Il pourrait cependant être intéressant de l'étendre à d'autres zones soumises à une plus forte convection libre, ceci donnant une estimation des conditions de réfraction dans la couche limite atmosphérique.

## TABLE OF CONTENTS

I.	INTRODUCTION . . . . .	10
II.	THE EXPERIMENT . . . . .	12
	A. LOCATION . . . . .	12
	1. Overview . . . . .	12
	2. Polar Queen Station . . . . .	12
	B. WEATHER CONDITIONS . . . . .	14
	C. MEASUREMENTS . . . . .	14
	1. In Situ Measurements . . . . .	15
	2. Sodar Measurements . . . . .	15
	D. GENERAL DATA REDUCTION. . . . .	16
	1. Determination of Surface Layer Scales Obtained from Surface Layer Similarity . . . . .	16
	2. Environmental Considerations for the Calculation of the Heat Flux . . . . .	17
	3. Calculation of $q^*$ . . . . .	19
	4. The Roughness Length . . . . .	20
III.	SODAR OPERATION AND ANALYSIS . . . . .	21
	A. DESCRIPTION OF THE SYSTEM . . . . .	21
	1. Basic Principles . . . . .	21
	2. Characteristics of the System . . . . .	22
	3. Dependence of the Received Signal on the Layer Stability . . . . .	23
	B. THE STRUCTURE FUNCTION AND THE TEMPERATURE STRUCTURE PARAMETER . . . . .	23
	1. Description . . . . .	23
	2. Surface Scaling . . . . .	24
	3. Sodar Data Reduction . . . . .	27
	C. REQUIREMENTS FOR SODAR CALIBRATION . . . . .	29
	D. COMPUTATION OF THE INVERSION HEIGHT . . . . .	31
	1. The Problem of Determining the Inversion Layer . . . . .	31

	2. The Inversion Layer Height . . . . .	32
	3. The Inversion Layer Thickness . . . . .	32
IV.	THE RESULTS . . . . .	34
	A. THE CALIBRATION OF THE SODAR . . . . .	34
	1. Analysis of the Results . . . . .	34
	2. Calibration of the System . . . . .	43
	3. Error Analysis . . . . .	46
	B. TIME-HEIGHT CROSS-SECTIONS OF THE INVERSION LAYER . . . . .	46
	1. 11 and 12 July . . . . .	47
	2. 13 July . . . . .	48
	3. 14 July . . . . .	54
	4. 15 July . . . . .	55
	5. 16 July . . . . .	55
	6. 17 July . . . . .	56
	C. ESTIMATION OF POTENTIAL TEMPERATURE JUMP AND REFRACTIVE-INDEX GRADIENT AT THE INVERSION LAYER . . . . .	56
	1. The Potential Temperature Jump . . . . .	56
	2. Refractive Index Gradient at the Inversion Layer . . . . .	58
	3. Comparison of some Results with Radiosonde Data . . . . .	62
V.	CONCLUSIONS AND RECOMMENDATIONS. . . . .	66
	APPENDIX A: COMPUTATION OF THE INVERSION LAYER HEIGHT USING SODAR DATA. . . . .	68
	APPENDIX B: TABLE OF ZI, QO, T*, DN/DZ AND $\Delta M$ . . . . .	72
	LIST OF REFERENCES . . . . .	75
	INITIAL DISTRIBUTION LIST . . . . .	78

*LIST OF FIGURES*

2.1	The Polar Queen Station . . . . .	13
4.1a	CT <sup>2</sup> versus Backscatter Intensity at Level 1 . . . . .	35
4.1b	CT <sup>2</sup> versus Backscatter Intensity at Level 2 . . . . .	36
4.1c	CT <sup>2</sup> versus Backscatter Intensity at Level 3 . . . . .	37
4.1d	CT <sup>2</sup> versus Backscatter Intensity at Level 4 . . . . .	38
4.1e	CT <sup>2</sup> versus Backscatter Intensity at Level 5 . . . . .	39
4.1f	CT <sup>2</sup> versus Backscatter Intensity at Level 6 . . . . .	40
4.2	CT <sup>2</sup> versus Backscatter Intensity at Levels 4, 5 and 6 . . . . .	44
4.3	Log(CT <sup>2</sup> ) versus Log(I) at Levels 4, 5 and 6 . . . . .	45
4.4a	Atmospheric Boundary Layer Structure on 11 and 12 of July . . . . .	48
4.4b	Atmospheric Boundary Layer Structure on 13 of July . . . . .	49
4.4c	Atmospheric Boundary Layer Structure on 14 of July . . . . .	50
4.4d	Atmospheric Boundary Layer Structure on 15 of July . . . . .	51
4.4e	Atmospheric Boundary Layer Structure on 16 of July . . . . .	52
4.4f	Atmospheric Boundary Layer Structure on 17 of July . . . . .	53
4.5	$\Delta M$ versus Time in the Inversion Layer. . . . .	60
4.6	Radiosonde Measurements for Two Different Times . . . . .	63
4.7	Display Terminal Shaded Plot around 1100Z on 14 July . . . . .	64

### *ACKNOWLEDGEMENTS*

I wish to acknowledge my advisor, Professor W.J. Shaw, for his support in conducting this thesis and for his worthy assistance. The data introduced here were gathered during the 1984 Marginal Ice Zone Experiment, and I thank Peter Guest for the information he acquired and shared with me. Thanks are also due to Lieutenant Mike Mohn of the U.S. Navy, whose programs allowed me some extra time in the analysis of the sodar data.

This thesis is dedicated to my next child expected in a few days.

## I. INTRODUCTION.

The atmospheric boundary layer (ABL), which is found just above the surface and generally extends to several hundred meters, can be considered to be composed of three different layers. At the lowest level is the surface layer, whose height is about one tenth of the ABL height and where turbulent exchanges with the surface are driven directly by vertical gradients. The mixed layer comprises most of the remaining ABL depth. Under unstable conditions mechanical and thermal mixing cause homogenous conditions. The third layer is the inversion layer where turbulent kinetic energy is small and there are strong vertical gradients. In particular, the gradient of potential temperature is associated with stronger fluctuations of the temperature.

The polar region is of particular interest because it is a region not only of scientific interest but also of military importance. This area differs significantly from the midlatitude and tropical ABL's, where anomalous electromagnetic propagation due to mean vertical gradient of temperature and humidity are frequently observed. Although anomalous propagation is not commonly reported in the Arctic Ocean, the boundary layer can extend to a low height and have a strong inversion layer. Another difference concerns the difference in the stability condition, with a generally more stable atmosphere at high latitudes and more convective conditions in mid-latitude or in the tropics. Therefore, it is important to understand the vertical structure of Arctic atmospheric boundary layer. To date, little work have has been done on this problem.

The Marginal Ice Zone experiment (MIZEX 84) was conducted in the summer of 1984 and produced a wealth of data with which to investigate the structure of the Arctic ABL. Several instrumented platforms were deployed in the East Greenland Sea during that

summer to measure the mesoscale processes that influence the advance and retreat of the ice margin. A variety of data were then gathered, including measurements of surface variables and sodar data. The sodar (Sound Detection and Ranging) system is one of the sensors used in this study. It measures the strength of the small-scale turbulence encountered along its vertical ray path. The intensity of the signal is proportional to the refractive-index structure parameter  $C_n^2$ , called also the structure function parameter, which has an important environmental influence on the propagation of electromagnetic waves. Profiles of this parameter provided by the sodar allow production of an image of the structure of the atmospheric boundary layer.

It is the purpose of this thesis to calibrate the sodar system deployed by the research vessel POLAR QUEEN during MIZEX 84 to obtain the refractive-index structure parameter. The time-height structure of the boundary layer will also be investigated. Efforts will also be made to compute the height of the inversion layer and to estimate its thickness, the jump of potential temperature, and the refractive-index gradient.



## II. THE EXPERIMENT

### A. LOCATION

#### 1. Overview

The recent phase of the Marginal Ice Zone Experiment was conducted during the summer of 1984. This experiment, which followed that of 1983, was designed to explore the drift, the formation, and the evolution of the ice margin through mesoscale processes.

The experiment began with a preparation period consisting mainly of satellite imagery analysis. Following this period, seven ships, eight aircraft and four helicopters belonging to the ten European and North-American countries involved in the experiment were deployed in Fram Strait area between Greenland and Svalbard Island (Spitsbergen). The first platform was on station at the beginning of June and the recovery period started on 17 July (Johannessen and Horn, 1984).

#### 2. Polar Queen Station

The main goal of the POLAR QUEEN was to follow the drifting motion of the ice. Therefore, she was moored to a floe a few kilometers inside the ice edge and drifted passively with the ice floe while various experiments were deployed to study the parameters which described the atmospheric boundary layer. Two different drifting phases occurred. The first one ended on 16 June when the floe was broken by the propagating swell generated by northerly winds. The station was then moved about 60 kilometers to the northwest and observations terminated on 17 July.

This most important part of the experiment was located in an area delineated by latitudes  $80^{\circ}\text{N}$  to  $81^{\circ}\text{N}$  and longitudes  $001^{\circ}\text{E}$

to 007°E. We will limit this study to the last week of the experiment from 11 July at 2150Z to 17 July at 1130Z where a most interesting data set was obtained. During this period the sodar display terminal showed a well formed inversion layer. This terminal produced a time-height cross section of the backscattered signal using shaded characters whose strength is proportional to the signal intensity. This gave a good *in situ* picture of the ABL structure.

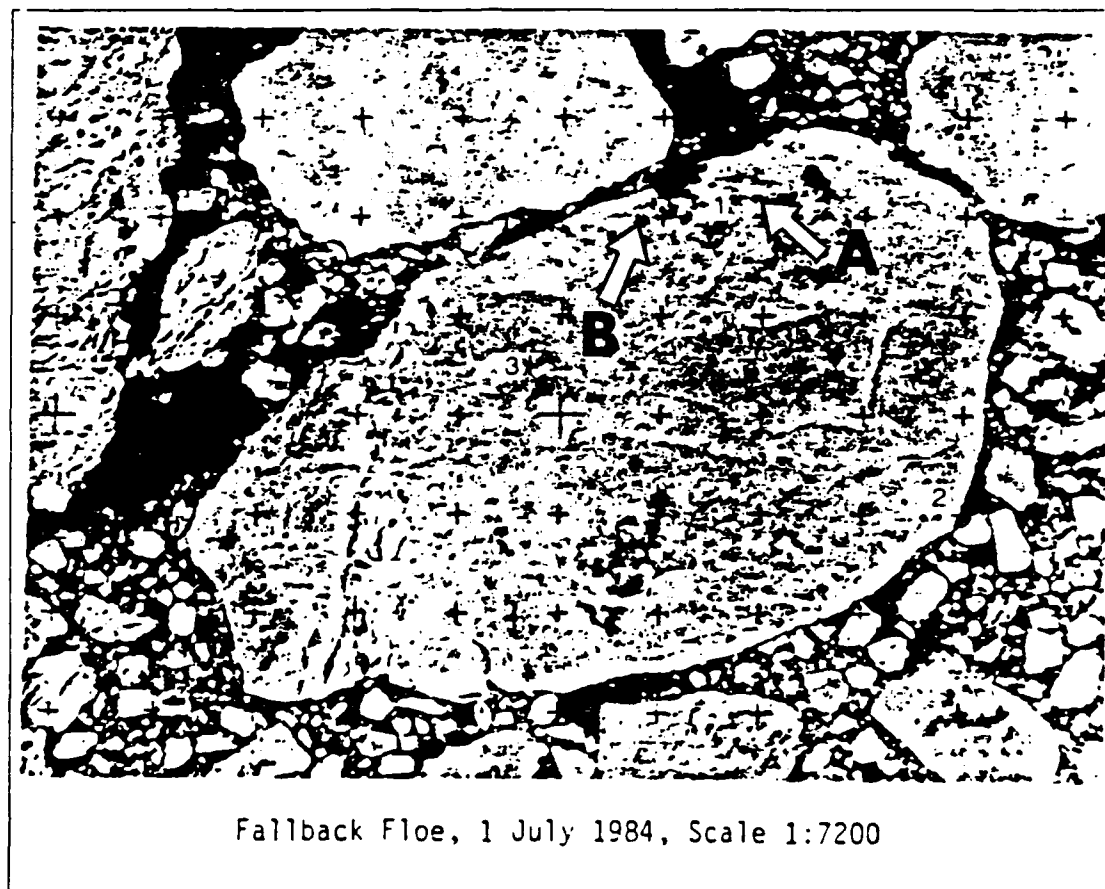


Figure 2.1 The Polar Queen Station.

The ship was moored on the port side to a large floe of approximately 400 by 700 meters as shown in figure 2.1. The POLAR QUEEN can be seen in dark, moored along the upper edge

of the main floe (named "Fallback floe"). As it can be seen in this picture, the surrounding region is composed of floes of a variety of sizes. The floes are all drifting, but not necessarily with the same motion. So the environment of the station varied, and this can induce variations in the heat and moisture flux depending on location. A parcel of air which is at a low height will be under the influence of the underlying ocean surface. A higher parcel can be affected by both ice and water surfaces.

#### **B. WEATHER CONDITIONS**

The weather was characterized generally by stratus or fog conditions, although there was less fog than during the 1983 experiment. Several low pressure systems passed through the region during the experiment. For the period of interest, the area was characterized by a high pressure system to the east of Svalbard Island. Another weaker high pressure center lay over Greenland, while a low pressure system was located north of Greenland to the northwest of the POLAR QUEEN station. These systems moved slowly and erratically. The pressure varied from 1004 millibars to 1020 millibars, with the minimum values occurring on about 11 July, with higher values later. No front crossed the area during that week. Winds were variable with velocities ranging from 0 to 15 m/sec.

#### **C. MEASUREMENTS**

The two different sources of the data to deal with were the *in situ* measurements and the sodar measurements.

## 1. In Situ Measurements

*In situ* measurements were obtained at two different locations. One was the ship itself, where surface pressure, air temperature, dew point temperature, wind speed and relative direction, and downward radiation were measured.

The second location was an ice mast located on the ice floe at about 50 meters from the edge as shown on figure 2.1 at spot "A". It provided air temperature and wind speed at different levels, from 5 cm to 5.3 m above the floe surface.

## 2. Sodar Measurements

To avoid noise interference from the ship, the SODAR system was installed on the floe at site "B" as is shown in figure 2.1, about 30 meters from the ice edge. It is expected that the acquired measurements were more influenced by surface ice than by the surrounding water.

The sodar system will be described in more detail in the next chapter. However, the system gave essentially a backscattered signal which is proportional to the small scale fluctuation of temperature in a layer encountered by the acoustic signal. These fluctuations influence the refractive index structure parameter  $C_n^2$ , which is mainly dependent upon the temperature structure parameter  $CT^2$ . This parameter is generally larger in the surface layer and in the inversion (or interfacial) layer. The sodar gave the values of the backscattered signal for each height at a rate of about one profile every minute. It will be possible to deduce the height of the inversion layer, and some information regarding its strength may be inferred. One goal of this study is to calibrate the sodar by computing the value of  $CT^2$  in the surface layer with only *in situ* measurements and then comparing these values with the sodar signal strength to obtain a calibration curve.

#### D. GENERAL DATA REDUCTION.

##### 1. Determination of Surface Layer Scales Obtained from Surface Layer Similarity

The *in situ* measurements include humidity and wind speed and temperature at different levels. From these  $U^*$ ,  $T^*$  and  $q^*$  may be obtained using:  $U^* = \langle -u'w' \rangle^{1/2}$ ,  $T^* = \langle -w'T' \rangle / U^*$  and  $q^* = \langle -w'q' \rangle / U^*$ . The bracket represents an average over time. These quantities were computed using the bulk method (Businger, 1973) derived from Monin-Obukhov similarity theory. A brief description of the method and results follows.

According to the bulk method, the following equations can be used to compute  $U^*$  and  $T^*$ :

$$U^* = kU'(z) / (\ln(Z/Z_0) - \phi_1(\xi)) \quad (2.1)$$

$$T^* = k\alpha(T - T_0) / (\ln(Z/Z_0) - \phi_2(\xi)) \quad (2.2)$$

where:

$k = 0.35$  von Karman's constant.

$\alpha = 1.35$  ratio of heat transfer to momentum transfer at  $\xi = 0$ .

$U'(z)$  (m/s) wind speed at height  $Z$ .

$Z_0, Z_{ot}$  roughness length for velocity and temperature profiles.

$\phi_1(\xi)$  and  $\phi_2(\xi)$  closed functions of the similarity height parameter  $\xi$ .

$\xi$  is defined as the ratio  $Z/L$  where  $L$  is the Monin-Obukhov length scale (Monin and Obukhov, 1954)

$$\xi = Z/L = Zkg (T^* + 6.1 \cdot 10^{-4} T q^*) / T U^{*2} \quad (2.3)$$

where  $g = 9.8 \text{ m/s}^2$  is the acceleration of gravity and  $q^*$  (gm/kg) is the water vapor mixing ratio scaling parameter.

$\xi$  was computed neglecting  $q^*$  because of the high relative humidity and low temperature which produce a low humidity gradient and, hence, a low value for  $q^*$ . Equation 2.3 becomes:

$$\xi = Zkg T^* / T U^{*2} \quad (2.4)$$

Equation 2.1 can be put in the form  $U(z) = m f(Z, \xi) + n$ , where  $f(Z, \xi)$  can be computed using an iteration process to get  $\xi$ .  $m = U^*/k$  is the slope of the curve and can be measured giving the value of  $U^*$ .  $n = U^* \ln(Z_0)/k$  is the intercept and allows the computation of  $Z_0$ . In fact, the drag coefficient was first computed using the formula:

$$Cd^{1/2} = U^*/U^{(10)} \quad (2.5)$$

where  $U^{(10)}$  is the wind speed at 10 meters. The range of "Cd" was found to be between 2.1 and 2.3  $10^{-3}$  m/s.

$T^*$  is compute in the same way as  $U^*$  and the two results produce the following transfer coefficient:

$$Ch = U^*T^* / U(z)(T-T_0)$$

where  $T^*/(T-T_0) = 0.032$  is obtained from a plot of  $T^*$  versus  $(T-T_0)$  This leads to:

$$Ch = 1.5 \cdot 10^{-3}$$

(Personal communication with P. Guest, 1985).

## 2. Environmental Considerations for the Calculation of the Heat Flux

The heat flux can be computed easily once we know  $U^*$  and  $T^*$

$$Q_0 = - U^*T^* \quad (2.6)$$

A summary of the most useful data for this study obtained from the *in situ* measurements and averaged over 15 values (about every 3 hours) are presented in Table I . Here the character "\*" means that there are no reliable data for the corresponding period.

TABLE I  
IN SITU AND REMOTE MEASUREMENTS

Date	Time	Temp °C	Rh. %	U <sup>10</sup> m/s.	P mbar.	U* m/s	T* °K	Q <sub>0</sub> °K (m/s)
11Jul	0453Z	0.3	99.1	4.8	1004.0	0.2270	0.0166	-0.0038
11Jul	0730Z	0.5	99.8	5.6	1004.1	0.2222	0.0205	-0.0054
11Jul	1002Z	0.3	98.8	5.0	1004.5	0.2229	0.0120	-0.0027
11Jul	1236Z	0.2	99.0	5.9	1004.9	0.2697	0.0094	-0.0025
11Jul	1509Z	0.0	98.1	5.5	1005.3	0.2504	0.0046	-0.0012
11Jul	1741Z	-0.2	97.7	4.7	1005.7	0.2065	0.0013	0.0003
11Jul	2027Z	-0.6	95.2	3.4	1006.7	0.1055	0.0086	0.0009
11Jul	2259Z	-0.4	90.2	2.7	1007.9	0.0653	0.0029	-0.0002
12Jul	0131Z	-0.6	89.9	2.1	1009.0	0.0583	0.0000	0.0000
12Jul	0402Z	-0.6	89.3	1.2	1010.0	0.0359	0.0089	0.0014
12Jul	0634Z	-0.9	88.9	1.4	1011.2	0.0618	0.0411	0.0025
12Jul	0906Z	-1.2	88.9	1.8	1012.2	0.0529	0.0864	0.0046
12Jul	1137Z	-1.0	88.9	2.2	1012.3	0.0626	0.1853	0.0116
12Jul	1411Z	-1.3	92.5	3.8	1013.3	0.0384	0.1944	0.0075
12Jul	1654Z	-1.5	94.8	3.2	1013.4	0.0210	0.0766	0.0016
12Jul	1927Z	-1.2	96.6	3.8	1013.3	0.1165	0.0434	0.0051
12Jul	2159Z	-0.7	99.7	3.8	1013.2	0.1009	0.0164	0.0017
13Jul	0032Z	-0.4	100.0	3.3	1012.7	0.1577	0.0124	0.0019
13Jul	0304Z	-0.1	100.6	2.2	1012.1	0.0309	0.0250	0.0008
13Jul	0535Z	-0.1	100.7	2.4	1011.5	0.0488	0.0175	0.0009
13Jul	0811Z	-0.1	100.7	2.8	1011.3	0.0765	0.0205	0.0016
13Jul	1042Z	-0.3	99.6	5.2	1011.4	0.1181	0.0432	0.0051
13Jul	1313Z	-0.2	99.3	6.2	1011.2	0.2978	0.0303	0.0090
13Jul	1544Z	-0.5	99.1	5.6	1011.5	0.2681	0.0327	0.0088
13Jul	1814Z	-0.5	100.3	3.9	1011.4	0.2706	0.0060	0.0016
13Jul	2045Z	-1.0	100.5	4.8	1011.8	*****	0.0047	*****
13Jul	2317Z	-1.2	99.9	5.0	1011.6	0.0689	0.0017	-0.0001
14Jul	0255Z	-1.1	99.4	4.2	1011.4	*****	0.0032	*****
14Jul	0522Z	-0.4	99.4	4.4	1011.5	0.2358	0.0024	0.0006
14Jul	0754Z	-0.8	99.4	4.8	1011.7	*****	0.0023	*****
14Jul	1025Z	-0.5	98.1	5.3	1011.7	0.0735	0.0319	0.0023
14Jul	1257Z	-0.6	98.5	5.3	1011.7	*****	0.0082	*****
14Jul	1529Z	-0.6	98.8	4.1	1011.6	0.0219	0.0090	0.0002
14Jul	1803Z	-0.2	99.8	6.0	1011.4	0.1264	0.0131	0.0017
14Jul	2034Z	-0.1	99.9	6.3	1011.5	0.1368	0.0019	0.0003
14Jul	2306Z	-0.0	100.6	3.3	1011.2	0.0872	0.0016	-0.0001
15Jul	0138Z	-0.2	99.3	6.6	1011.2	0.2367	0.0015	0.0003
15Jul	0409Z	-0.4	95.7	7.2	1011.2	0.3067	0.0095	-0.0029
15Jul	0641Z	-0.1	99.9	7.4	1011.6	0.3020	0.0015	-0.0005
15Jul	0913Z	-0.0	99.5	6.8	1012.1	0.2702	0.0019	-0.0005
15Jul	1144Z	-0.2	98.0	6.6	1012.4	0.2972	0.0081	0.0024
15Jul	1416Z	-0.3	93.7	7.4	1012.8	0.3306	0.0117	0.0039
15Jul	1741Z	-0.6	97.9	7.0	1013.3	0.3024	0.0205	0.0062
15Jul	2102Z	-0.4	94.8	7.0	1013.8	0.3140	0.0072	0.0023
15Jul	2334Z	-0.1	99.1	6.2	1014.4	0.2397	0.0164	-0.0039
16Jul	0207Z	-0.5	97.9	5.9	1014.7	0.2544	0.0281	-0.0072
16Jul	0439Z	-0.8	98.6	5.4	1015.0	0.2316	0.0297	-0.0069
16Jul	0746Z	-1.2	99.8	4.7	1015.6	0.1991	0.0408	-0.0081
16Jul	1017Z	-1.3	99.9	4.7	1016.3	0.2077	0.0420	-0.0087
16Jul	1248Z	-1.5	98.5	5.3	1016.7	0.2104	0.0486	-0.0102
16Jul	1519Z	-1.5	99.3	5.4	1016.9	0.1910	0.0486	-0.0093
16Jul	1750Z	-1.7	99.2	6.4	1017.0	0.1804	0.0487	-0.0088
16Jul	2021Z	-1.7	99.4	6.8	1017.3	0.2056	0.0572	-0.0117
16Jul	2251Z	-1.7	99.8	7.4	1017.8	*****	*****	*****
17Jul	0122Z	-1.9	99.5	7.9	1018.1	*****	*****	*****
17Jul	0354Z	-2.2	98.2	8.5	1018.3	*****	*****	*****

REPRODUCED AT GOVERNMENT EXPENSE

A question which arises at this point is: "What was the relative influence of the sea and of the ice on the computation of  $U^*$  and  $T^*$ ?" For the ice mast, there was nearly no influence of sea water because the measurements are taken close to the floe surface. However for the ship, which was in the water surrounded by scattered pieces of ice, the problem may be more complex. The surface of the ice can be considered to be nearly at the same temperature as the sea water, close to  $273^\circ\text{K}$ . It can also be assumed that the humidity of the ice surface was nearly equal to 100 % because of a generally thin skin of melting ice and snow on the floes, which more or less resembled large ponds of water in this last part of the experiment. Therefore, there will be no effort to separate the influences from water and from ice in the derivation of  $U^*$ ,  $T^*$ ,  $q^*$  and  $Q_0$ .

### 3. Calculation of $q^*$

Assuming that the previous coefficient  $Ch$  can be applied to the formula which gives  $q^*$ , it is possible to examine the assumption that the effects of  $q^*$  are negligible. An alternative way to express  $q^*$  and  $T^*$  is the following:

$$T^* = c^{1/2} (T - T_0) \quad (2.7)$$

$$q^* = c^{1/2} (q - q_0) \quad (2.8)$$

where " $q$ " and " $q_0$ " are the specific humidity at 10 meters and at the surface respectively. " $c$ " is the drag coefficient and is related to  $Ch$  by:

$$c^{1/2} = Ch U^{(10)}/U^* \quad (2.9)$$

If the drag coefficients are the same for  $q^*$  and  $T^*$ ,  $q^*$  can be expressed by:

$$q^* = 1.5 \cdot 10^{-3} U^{(10)}(q - q_0) / U^* \quad (2.10)$$

$(q - q_0)$  is computed using Clausius-Clapeyron equation (Fleagle and Businger, 1980):

$$q - q_0 = \exp[(9.4 - 2353/T) \ln 10] (Rh/100 - 1) 0.622/P \quad (2.11)$$

Here  $P$  is the pressure in millibars and  $Rh$  is the relative humidity on the ship. The measurement is assumed to apply to a height of 10 meters. The relative humidity at the surface was taken to be 100% because of the large ponds of water on the ice floe and the melting snow as stated previously.

The magnitude for  $T^*$  was between  $10^{-1}$  °K and  $10^{-2}$  °K while  $6.1 \cdot 10^{-4} T q^*$  goes from  $10^{-5}$  to  $10^{-5}$  g/kg. So this term can, in fact, be neglected in equation 2.3 .

#### 4. The Roughness Length

Assuming that  $C_d$  is measured close to neutral stability we have:

$$C_d^{1/2} = k / \ln(Z/Z_0) \quad (2.12)$$

which leads to:

$$Z_0 = Z \exp(-k / C_d^{1/2}) \quad (2.13)$$

for  $Z = 10$  meters and  $C_d = 2.2 \cdot 10^{-3}$ , we get:

$Z_0 = 2$  millimeters. This value is greater than the usual quantity for the roughness length, probably because of the irregularity of the ice surface.

### III. SODAR OPERATION AND ANALYSIS

#### A. DESCRIPTION OF THE SYSTEM

##### 1. Basic Principles

The acoustic sounder operates much like a classical radar but emits an acoustic rather than an electromagnetic pulse in a narrow beam and receives a signal which comes from scattering of the acoustic wave by air parcels at various levels. This backscattered signal is due to small-scale acoustic refractive index inhomogeneities which are the consequences of local fluctuations of the air temperature and velocity. The effects of the humidity fluctuations are negligible because they do not affect significantly the sound velocity fluctuations, which are directly related to the changes in index of refraction (Parry *et al.*, 1972). This will be verified later.

A monostatic sodar system uses an antenna configuration in which the transmitters and receivers are co-located. Thus, the received signal is due to direct backscatter. Since the velocity variations produce a maximum scattering in the forward direction and do not contribute to backscattering, the received intensity will not depend on the air velocity fluctuations and will be mainly a function of the local temperature variations. These are described by the temperature structure parameter " $CT^2$ ". Since temperature fluctuations are largest in the surface layer and in the inversion layer of an unstable ABL, there will be maximum backscattered signal intensity in these regions.

## 2. Characteristics of the System

The system emits a 100 ms pulse at a frequency  $f = 2$  kHz and then shifts to reception mode for a few seconds. This time is variable, depending on the height being probed. The listening period is divided into several segments or "bursts" of 4 ms, each which will represent a certain distance covered by the signal. To have a complete representation of the vertical layer above the antenna, the total sounding depth is divided into altitude intervals called "gates" which are characterized by a certain number ( $n$ ) of bursts. An average is made for each gate to give the final backscattered signal. The altitude interval  $d$  of the gates is manually variable by changing the number  $n$ . The value of  $d$  is then given by the formula:

$$d = 4 \cdot 10^{-3} n V / 2, \quad (3.1)$$

where  $V$  is the speed of sound in the atmosphere and is approximated by the formula:

$$V = 20 T^{1/2} \text{ m/s}$$

where  $T$  is the absolute temperature of the medium. For  $T = 273^\circ\text{K}$  we get  $V = 331$  m/s, which was used to determine the height scale. Consequently, for a gate of 7 bursts, the interval will be  $d = 4.6$  meters. There are 200 gates for each profile which can cover a height of  $25 + (200 \cdot 4.6) = 945$  meters which will be a maximum height of the backscattered profiles. The measurements begin at 25 meters because of transmitter ringing and antenna near-field effects.

Another parameter of interest is the wavelength of the signal which is given by:

$$L = V/f = 16.5 \text{ cm}$$

The most important scattering by small scale fluctuations is done by eddies whose size is half the wave length (about 8 cm in our case) of the acoustic wave (Parry *et al.*, 1975).

### 3. Dependence of the Received Signal on the Layer Stability

The backscattered signal depends on the small scale inhomogeneities encountered, which are related to the atmospheric boundary layer structure and stability.

#### a. Unstable Mixed Layer

Hydrostatic instability occurs when the surface temperature is larger than the temperature of the layer above. This induces upward (positive) buoyancy flux (and heat flux  $Q_0$ ). The resultant mixing extends to the interfacial layer. Then the potential temperature away from the surface becomes more homogeneous and its variations with height are reduced, producing less backscattering. The highest values of the backscatter signal level will be in the surface layer and in the interfacial layer where the vertical gradients of temperature are much greater.

#### b. Stable Boundary Layer.

When the surface temperature is smaller than the air temperature, there are downward (negative) buoyancy flux and heat flux. This tends to establish a less neutral lapse rate above the surface and to increase the temperature variance. In this case, the small-scale refractive index variations are stronger, and the backscatter signal level will be larger.

## B. *THE STRUCTURE FUNCTION AND THE TEMPERATURE STRUCTURE PARAMETER*

### 1. Description

The refractive index gradient produced by the interaction of the acoustic wave with small scale velocity fluctuations is expressed by the structure function  $D_n(r)$  which is defined by:

$$D_n(r) = \langle [N(x) - N(x+r)]^2 \rangle. \quad (3.2)$$

Here  $N$  is the index of refraction at two points in space separated by a vectorial distance  $r$ . The bracket represents an average over all space. Small-scale turbulence theory predicts that the structure function value is determined by the structure parameter  $C_n^2$  and the scalar separation " $r$ " by the formula:

$$Dn(r) = C_n^2 r^{2/3} \quad (3.3)$$

This is valid only if the magnitude of  $r$  lies within the inertial subrange of the turbulence, so that isotropy is "locally" valid.

Including both the temperature and water vapor contributions, the structure function is related to the temperature structure parameter  $CT^2$ , to the humidity structure parameter  $Cq^2$  and to the temperature-humidity structure parameter  $Ctq$  by:

$$C_n^2 = (79 \cdot 10^{-6} P/T^2)^2 (CT^2 + .113 Ctq + 3.2 \cdot 10^{-3} Cq^2), \quad (3.4)$$

where  $P$  is the pressure in millibars and  $T$  the absolute temperature (Friehe, 1977).

## 2. Surface Scaling

The structure parameters can be related to the measured meteorological quantities through Monin-Obukhov surface layer similarity parameters (Wyngaard, *et al.*, 1971 and Wyngaard, 1973).

$$CT^2 = T^{*2} Z^{-2/3} f(\xi) \quad (3.5)$$

$$Cq^2 = A Q^{*2} Z^{-2/3} f(\xi) \quad (3.6)$$

where  $f(\xi)$  is the empirical function found by Wyngaard, *et al.* and updated by Davidson *et al.* (1978). The quantity " $A$ " is a constant approximately equal to 0.6 (Fairall, *et al.* 1980) The temperature-humidity structure parameter is given by:

$$Ctq = R T^* Q^* Z^{-2/3} A^{1/2} f(\xi) \quad (3.7)$$

where "R" is the temperature-humidity correlation parameter (approximately 0.8 under unstable conditions). The value of R is not well known in the surface layer.  $Q^*$  is the water vapor density scaling parameter ( $\text{gm/m}^3$ ) and is related to  $q^*$  by:

$$Q^* = \rho q^*$$

Where  $\rho = 1.2 \text{ kg/m}^3$  is the air density.

The Monin-Obukhov length scale was defined by equation 2.3 and was approximated, neglecting the  $q^*$  contribution, by equation 2.4, which is repeated here:

$$\xi = Z/L = ZkgT^* / T^{2*} \quad (3.8)$$

The function  $f(\xi)$  has different forms for unstable ( $\xi < 0$ ) and stable ( $\xi > 0$ ) conditions and is a constant for neutral ( $\xi = 0$ ) conditions:

$$f(\xi) = 4.9(1 - 7\xi)^{-2/3} \quad (\xi < 0: \text{unstable}) \quad (3.9)$$

$$f(\xi) = 4.9 \quad (\xi = 0 : \text{neutral}) \quad (3.10)$$

$$f(\xi) = 4.9(1 + 2.4\xi^{2/3}) \quad (\xi > 0 : \text{stable}) \quad (3.11)$$

The problem of predicting  $Cn^2$  is therefore reduced to finding values of  $q^*$ ,  $T^*$  and  $U^*$ . The ratio  $CT^2/Cq^2$  shows the relative importance of  $T^*$  and  $q^*$ :

$$CT^2 / Cq^2 = T^{*2} / A Q^{*2}. \quad (3.12)$$

This gives:

$$CT^2 / Cq^2 = T^{*2} / 0.6 (1.2 q^*)^2 = 1.4 T^{*2} / q^{*2}$$

In equation 3.4 there is a factor equal to  $3.2 \cdot 10^{-3}$  between the contribution of the  $CT^2$  and the  $Cq^2$  terms. Therefore the contribution of  $Cq^2$  may be significant (more than 5%) if

$$3.2 \cdot 10^{-3} Cq^2 / CT^2 > 5\%.$$

This leads to:

$$1.4 T^{*2} / q^{*2} = CT^2 / Cq^2 < 3.2 \cdot 10^{-3} / 5\%$$

Thus the final condition is :

$$T^* / q^* < 0.2^\circ K / (g/kg).$$

For a 10 % contribution, the ratio should be less than 0.1. This means that  $q^*$  should be greater than 10 times the value of  $T^*$  if its influence is significant. It is known already that we do satisfy the necessary condition for this ratio, and the value of  $Cq^*$  can be neglected in equation 3.4. The same result will be found for the contribution of  $Ctq$ , even with the imprecision concerning "R".

The next step is to use equations 3.9 through 3.11 in equation 3.5 to get  $CT^2$  in the surface layer for every kind of stability:

$$CT^2 = 4.9T^{*2}Z^{-2/3}(1-7\xi)^{-2/3} \quad \xi < 0 \quad (3.13)$$

$$CT^2 = 4.9T^{*2}Z^{-2/3} \quad \xi = 0 \quad (3.14)$$

$$CT^2 = 4.9T^{*2}Z^{-2/3}(1+2.4\xi^2)^{2/3} \quad \xi > 0 \quad (3.15)$$

These three final equations will allow to determine the value of  $CT^2$  in the surface layer with only the *in situ* data. In certain circumstances it is possible to measure  $CT^2$  directly by measuring the variance of the temperature at different points in the atmosphere, but this was not done for the data for this study.

### 3. Sodar Data Reduction

#### a. The Data Set

The sodar data, which include sodar characteristics and measurements, were recorded on an 8-inch floppy disk and subsequently transferred to 9-track magnetic tapes which can be used with the NPS IBM 3033 mainframe computer. One tape contains the data for the period going from 11 July at 2150Z to 12 July at 1100Z and another tape the remaining data from 13 July at 0230Z to 17 July at 1130Z. Unfortunately, there are some gaps in the data set due to technical problems during the transfer.

(1) Time. The date and time are first obtained. Some profiles are missing because of computer "interfacing" difficulties, and the interval separating two profiles can vary a little during each day. This aspect does not change the reliability of the measurements corresponding to each time. The only problem this generates is in the averaging process, which will be discussed in section B.3.b.

(2) Gate and Altitude. Each profile gives a value proportional to backscattered sound intensity at different heights for the same time. The tape gives the value of a burst which is always equal to 4 ms in our case. It also provides the number of bursts per gate, which allows computation of the altitude for each gate. This interval was constant and corresponded to 7 bursts/gate for the first tape (11 and 12 July), which gives an interval of 4.6 meters as shown earlier. For the second tape it varies from 2 to 6 bursts/gate. This gives an interval between 1.3 and 4 meters from equation 3.1. The maximum heights detectable for these cases were, respectively, 290 and 820 meters. To simplify the data set of the second tape, it was necessary to make a transformation in the signal intensity for each profile and each level and to normalize the interval everywhere. A 5 bursts/gate interval was chosen because it was the value encountered most of the time (and the

closest to the other numbers), so that the mathematical transformation causes as little imprecision as possible.

(3) Noise and Signal.. A background noise estimate is obtained during each profile and is subtracted from the backscattered intensity, after some corrections which depend on gate altitude. These final power values become the usable data for each level after an averaging process is executed by the system for each profile and each gate.

Additional noise can be caused by aircraft or helicopter operations. Because the gain of the system is rather high, it is very sensitive to any external noise sources. The air flow around the acoustic enclosure can also produce noise. This was most likely when the wind speed was higher than 9 m/s.

When the system detected noise in excess of an adjustable threshold, it simply assigned an arbitrary value to the backscattered signal intensity of  $I = 32767$ , whereas usual values were between 200 and 600.

#### b. The Averaging Processes

Because of the sometimes important fluctuations of the received signal, it was necessary to smooth the response with an averaging technique. For this process as well as for the plot of the boundary layer, the programs were adapted from those of Lt. Mohn (1985). The first step of the analysis was to read the profiles by groups of eight and make an average for each gate. Then we have a value of the backscatter signal ranging from every 7 to 10 minutes. This range is variable for a given day and increases until 10-15 minutes for the last two days. As discussed earlier, the averaging interval is not constant. On a particular day, there is not much discrepancy from an arbitrary constant interval. However, there are two periods which will be the object of some comments in the time-height cross-section of the boundary layer's section.

### C. REQUIREMENTS FOR SODAR CALIBRATION

The method to retrieve  $CT^2$  implies the calibration of the system in order to obtain a relation of the form:

$$CT^2 = f(I)$$

As  $CT^2$  and  $I$  should be proportional, it is expected to find a linear function of the first order for  $f(I)$ . To find it,  $CT^2$  is computed in the surface layer using equations 3.13 to 3.15. This will be done for the first six levels, whose height goes from 25 m to 41.5 m with a separation of 3.3 m given by equation 3.1, when there are 5 bursts per gate. This was not the case for the first tape, but after elimination of data which do not fit for this computation, only one pair of data remained whose value of  $CT^2$  comes from this tape.

In the next step a program plotting  $CT^2$  versus  $I$  is used for the six different heights. To get good data for each set, the  $CT^2$  values are averaged for about every half hour. As the values of the *in situ* measurements are already averaged every 10 minutes, 3 values are averaged, keeping the time of the middle value. Then the values of the backscattered signal are read 15 minutes before and after this time and averaged to complete the set of two values ( $CT^2$ ,  $I$ ).

The quality of these pairs must be evaluated before generating a  $CT^2 = f(I)$  relation, following some criterion:

- The height of the level considered in the surface layer must be less than 1/10 of the height of the inversion layer for the equations giving  $CT^2$  in the surface layer to be still valid. As will be seen in figure 4.4b, there was an interesting evolution of the inversion layer on 13 July. But this does not help very much to get favorable sets of data because the inversion layer height is always below 250 m from 1100Z to 1700Z.

- For the same reason, if a second mixed layer forms from the ground and so is very low, or if we have a stronger signal at

intermediate level, the 6 levels considered will be probably higher than 1/10 this new height. Therefore, these data which correspond to a level which is above the surface layer must be rejected.

For example, on 13 July from 0300Z to 1100Z it will be seen in figure 4.4b , a second inversion layer whose height varies from the ground to 230 meters. The display terminal shows also the same kind of phenomenon on 14 July at 0330Z when a second inversion layer begins to rise up from the surface layer, reaching a height of about 150 meters at 0430Z and 200 meters at 0530Z. Then it is completely mixed with the surface layer at 0600Z. Also on 16 July, a new layer forms at 0300Z at a height of about 250 meters. Then it lowers to 100 meters at 0415Z before joining the surface layer.

During all these periods, the corresponding sets of values must be eliminated when the height of the inversion layer is too low (below 250 meters) and cannot fit with the 1/10 rule's requirement because the sodar cannot make any measurement below 25 m.

Another source of problems is the fact that there are some gaps in the data set of the *in situ* measurements made from POLAR QUEEN station. This led to missing values for  $U^*$ . About half of these values are missing between 11 July at 2300Z until 14 July at 2300Z. Also  $T^*$  and  $U^*$  are not known from 16 July 2100Z until the end of the measurement period. Therefore, it is not possible to form pairs of data for the calibration during these intervals of time.

In the backscatter signal data there are also bad data due to noise. There are relatively few such cases, and they are generally encountered at the first level. For instance, on 14 July from 1315Z until 1700Z, about half of the data set at the first level is unusable, but there are still enough values left for the averaging process; which is done about every half hour and during which 25 profiles are read.

Since  $CT^2$  and  $I$  are obtained in the surface layer for 6 levels, it is possible to calibrate the system after having deduced the function relating  $CT^2$  and  $I$  at these low levels. After that the

value of the backscattered signal needs to be used with this relation to get the value of  $CT^2$  everywhere in the atmospheric boundary layer.

#### *D. COMPUTATION OF THE INVERSION HEIGHT*

It is possible to compute the inversion layer height  $Z_i$  with the data set without generating a time-height cross-section. To do that it is only assumed that the inversion height occurs when the backscattered signal is maximum outside the surface layer. There are some difficulties if there are two different inversion layers or if the boundary layer is stable and produces a substantial return throughout.

##### 1. The Problem of Determining the Inversion Layer

The problem of multiple inversions is not too disturbing because a second inversion layer is generally weaker and is not accounted for in the algorithm.

The second problem is more troublesome. The strength of the signal just above the surface may be stronger than the interesting signal. In that case, it is necessary to read the data not at the first level, but at a higher one, where the strong surface layer return is not included. Sometimes this extension from the surface reaches higher than the inversion layer itself. Therefore, the first level to be considered must be determined, depending on the particular configuration for a given day or part of day. If not, the result will indicate either the top of the surface layer or the inversion layer, or even a height above the inversion if the first level considered is above the inversion.

The program must be run a few times to determine the first appropriate level to be read with regard to a particular interval of time. This first level will be adjusted and changed in

order to be always approximately between the surface layer and the inversion layer.

## 2. The Inversion Layer Height

Once this difficulty is solved, the height of the inversion is computed using two averaging processes. The first one, as before, consists of averaging the backscattered signal for each level, taking eight profiles over a time of about ten minutes.

The second process gives the height of the stronger signal and is executed by making a running vertical average which spans five levels. The stronger value obtained will give the level of the inversion layer.

## 3. The Inversion Layer Thickness

Another useful feature which can be computed from the sodar data is the inversion layer thickness. This is done in the same program that gives the inversion layer height. The averaging processes are the same, but instead of searching for the strongest vertical signal, we look for the weakest signal below the inversion, which should occur where the structure function parameter is the smallest. This happens generally at the base of the inversion layer  $Z_l$ . To find the value of the top of the inversion layer  $Z_u$ , the level above  $Z_l$  is determined where the averaged value of the signal is half of its maximum. This factor  $1/2$  is arbitrarily chosen, but since the value of the signal decreases relatively fast above the inversion than below, a strong change of the signal will occur for a small height difference. Therefore, the imprecision in choosing this factor should not be important.

The final value  $Th$  of the inversion thickness is given by:

$$Th = Zu - Zl \quad (3.16)$$

A listing of this program with some comments is given in Appendix "A".

## IV. THE RESULTS

In this chapter, we will look at the three different kinds of results obtained with the methods described previously: the calibration of the sodar, the time-height cross-section history for MIZEX-84, and the estimation of the potential temperature and the refractive index gradient in the inversion layer.

### A. THE CALIBRATION OF THE SODAR

#### 1. Analysis of the Results

Figure 4.1 shows  $CT^2$  versus  $I$  for the six backscatter levels closest to the surface. Specifically these are:

- Figure 4.1a : level 1 , 25 meters.
- Figure 4.1b : level 2 , 28.3 meters.
- Figure 4.1c : level 3 , 31.6 meters.
- Figure 4.1d : level 4 , 34.9 meters.
- Figure 4.1e : level 5 , 38.2 meters.
- Figure 4.1f : level 6 , 41.5 meters.

##### a. Level 1

The first plot seems to be unreliable because all the values of  $I$  are in the same range, whatever the value of  $CT^2$ . The reason may be related to effects of transducer reverberation on the gates which are the closest to the sodar system. This is suggested by the fact that a lot of values for  $I$  equal to 32767 are encountered at this level, an indicator of signal saturation. An interesting feature is the asymptotic approach to  $I=480$  that the curve appears to have as  $CT^2$  increases. Before making any comment, the other levels shall be examined.

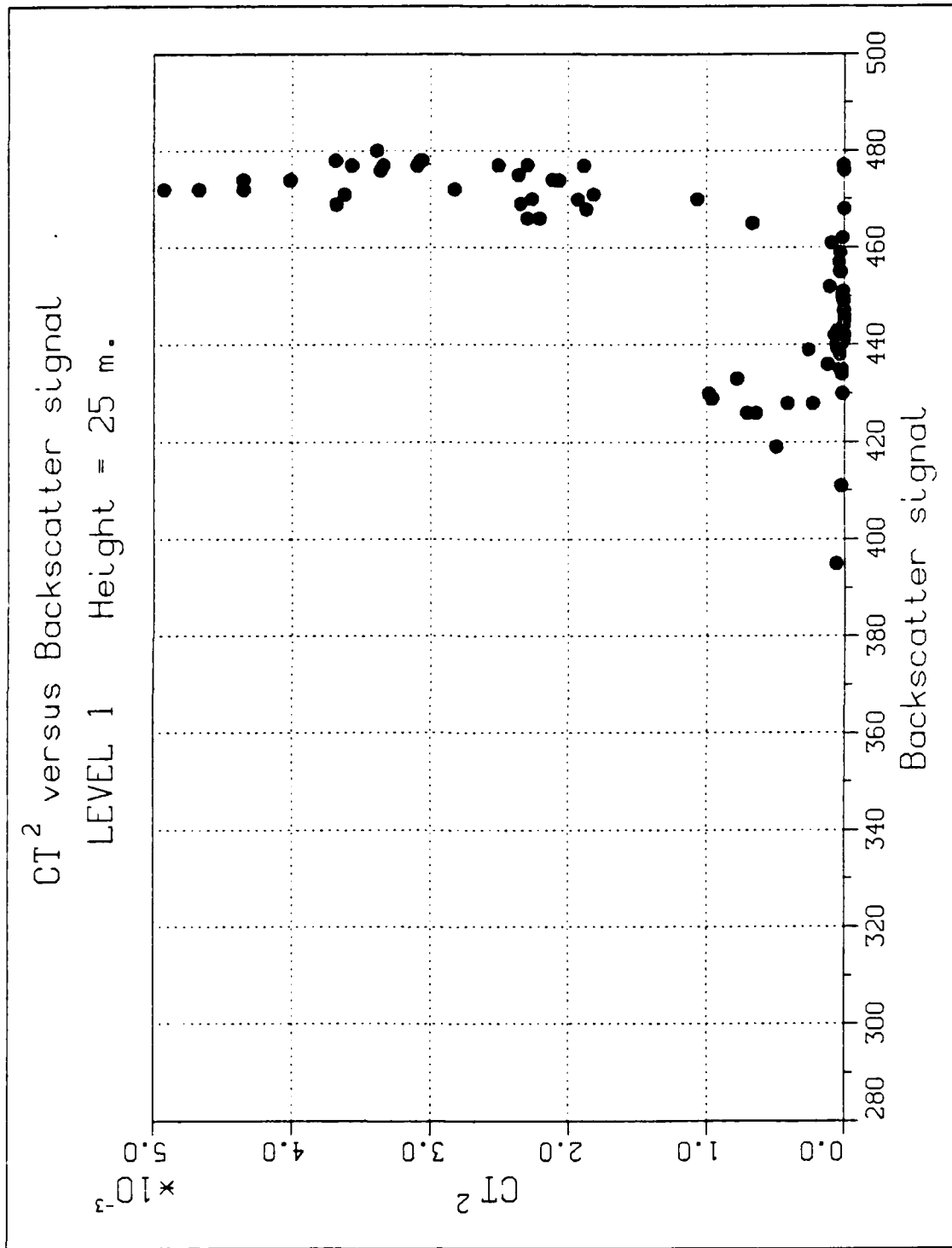


Figure 4.1a CT<sup>2</sup> versus Backscatter Intensity at Level 1.

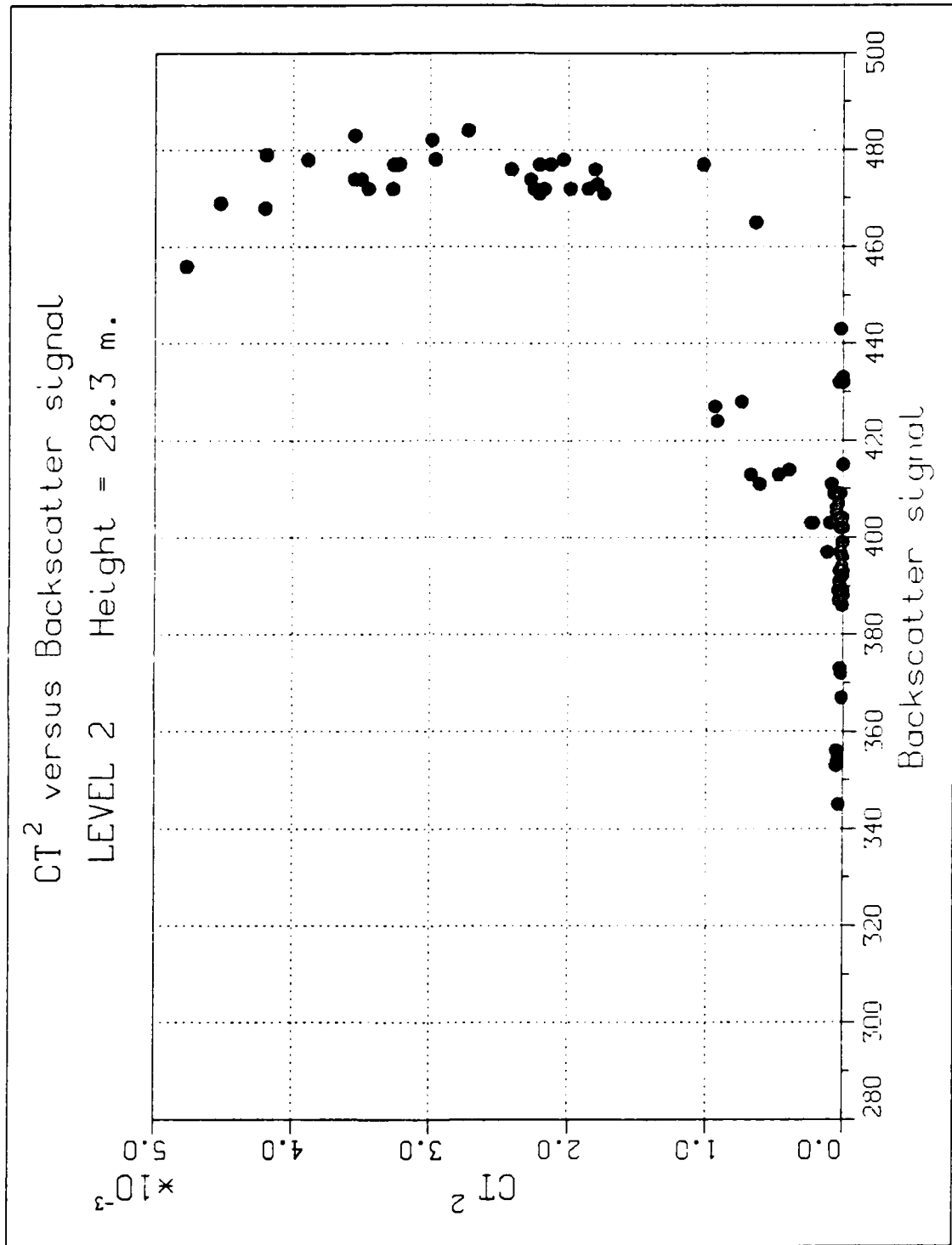


Figure 4.1b CT<sup>2</sup> versus Backscatter Intensity at Level 2.

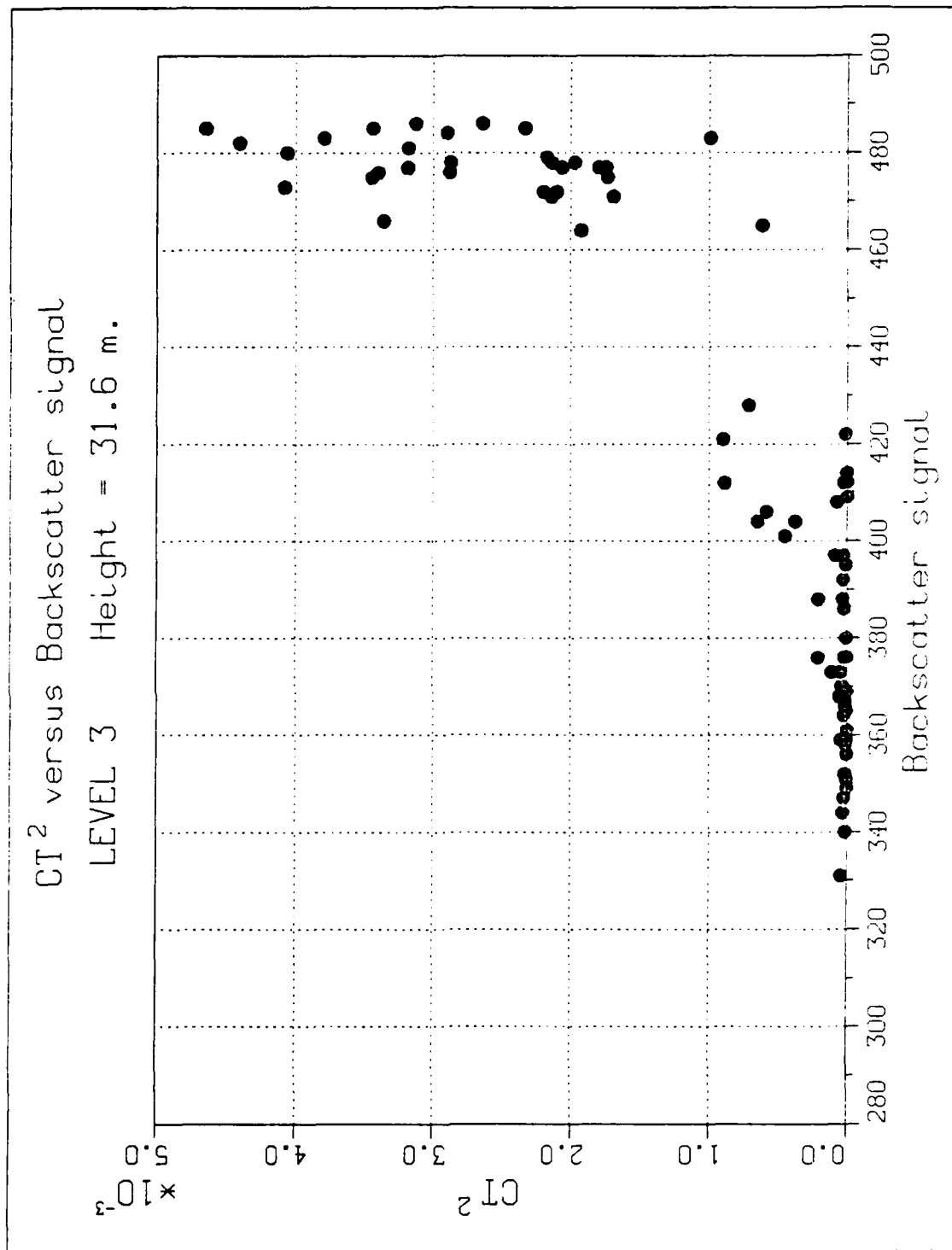


Figure 4.1c CT<sup>2</sup> versus Backscatter Intensity at Level 3.

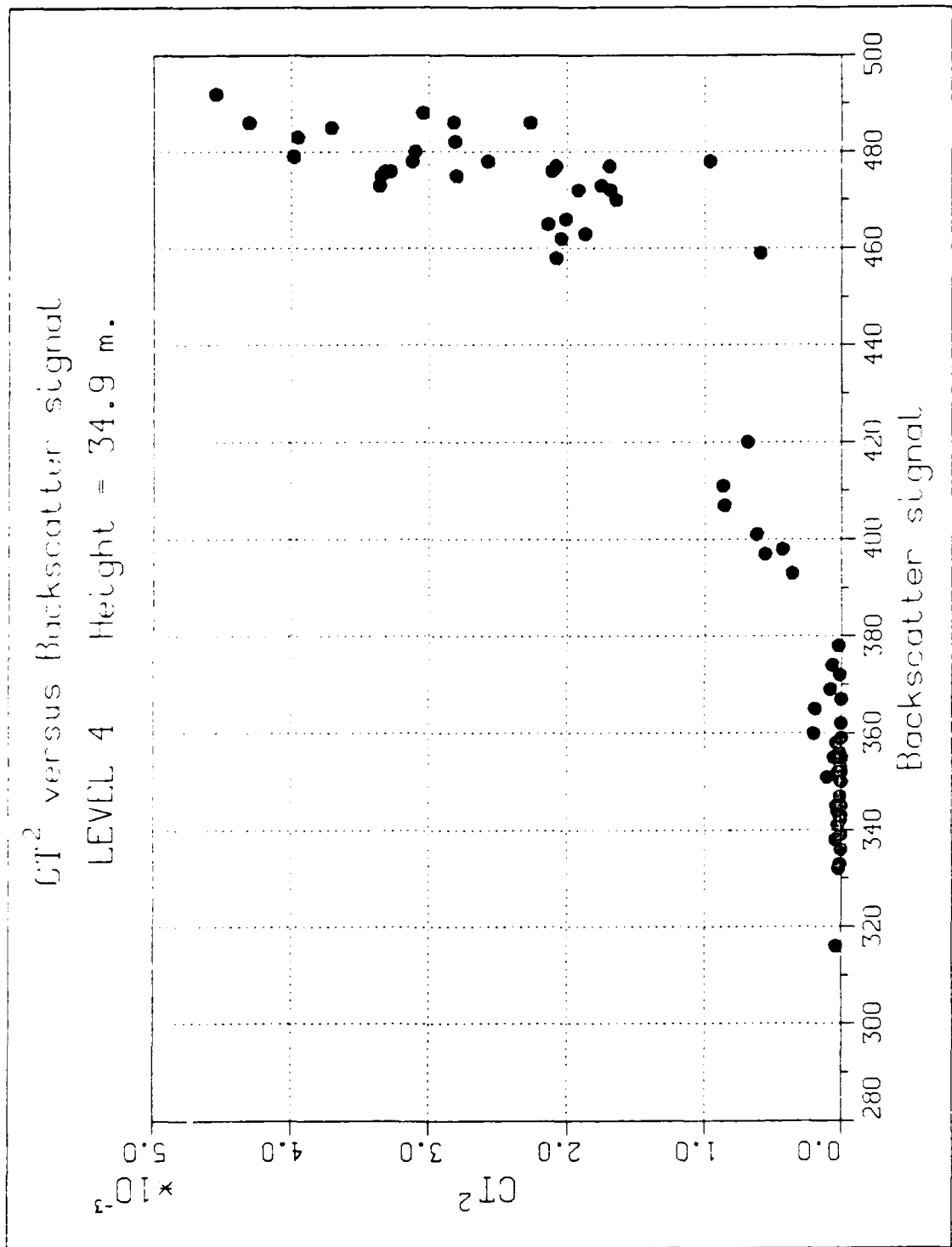


Figure 4.1d CT<sup>2</sup> versus Backscatter Intensity at Level 4.

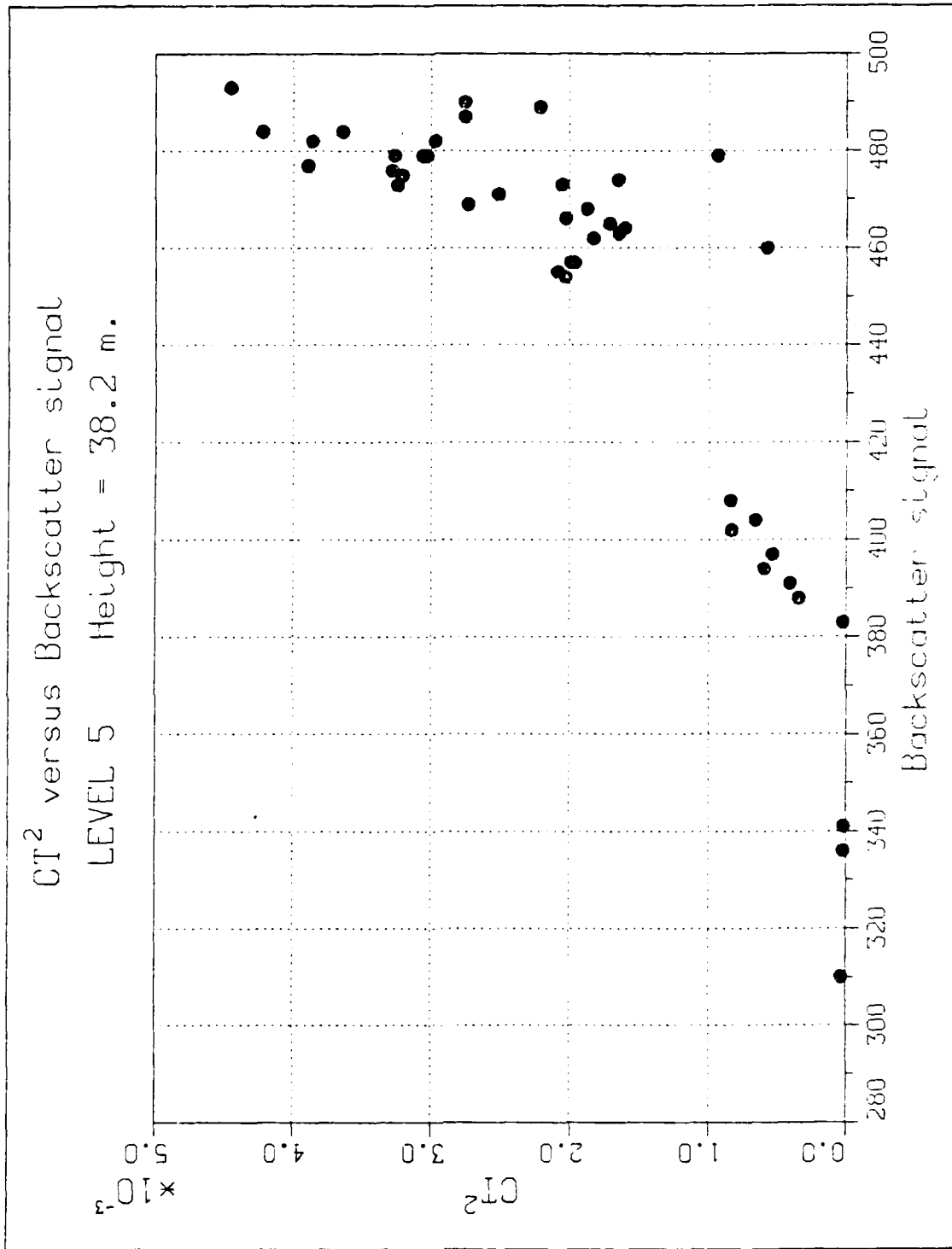


Figure 4.1e  $CT^2$  versus Backscatter Intensity at Level 5.

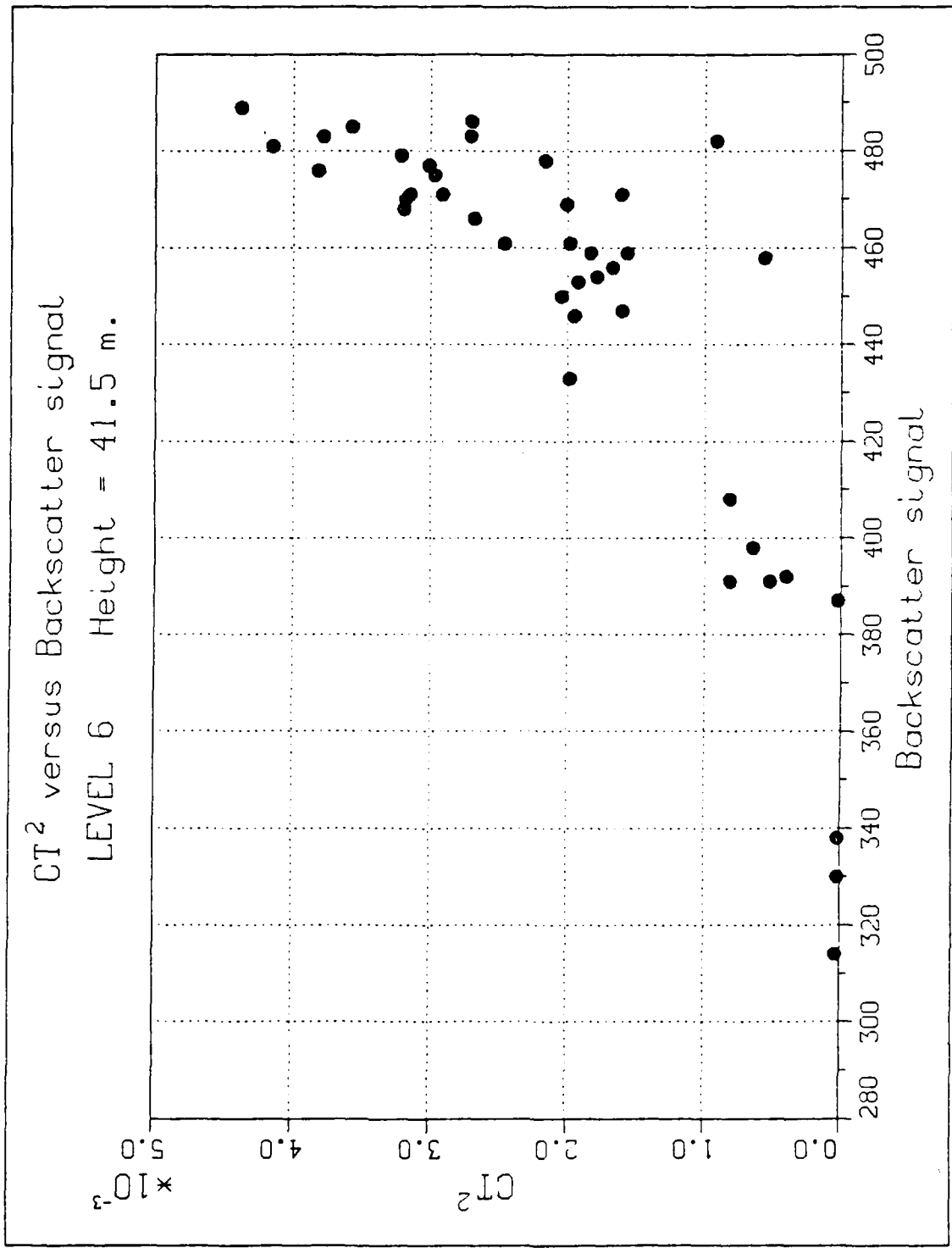


Figure 4.1f CT<sup>2</sup> versus Backscatter Intensity at Level 6.

b. Level 2

This level, shown in figure 4.1b, looks rather like the former one. The reverberation still appears to be significant at this range, although for small values of  $CT^2$ , the intensity is lower than before. There is evidence of a monotonic functional dependence of  $CT^2$  on  $I$  for  $400 < I < 475$  ( $CT^2 = 10^{-4}$ ,  $I = 400$ ) to ( $CT^2 = 2 \cdot 10^{-3}$ ,  $I = 475$ ). After that point there is, as before, a limitation which looks like a saturation of the system at  $I = 485$ .

c. Level 3

The lower points spread a little more than previously and the starting point of the curve seems to be at  $I = 370$ .

A few points seem to be out of range:

- There are five of them in the area delineated by  $0 < CT^2 < 10^{-4}$  and  $408 < I < 422$ . One of these points is taken on 14 July at 1712Z, when the inversion layer is about at 320 meters for the half hour average. This value is at the limit of ten times the height of level 3 (31.6 m), and therefore the bulk formula calculation of  $CT^2$  may be tenuous. It may also be due to non-stationarity, in which case the fluxes may no longer be constant with height and the similarity theory no longer holds. Advection of heat and velocity may play a similar role, which invalidates similarity theory by changing the balance of the terms in the equations of motion.

On 15 July the other points span the time from 0923Z to 1024Z and occur at 1528Z when the inversion height is between 310 and 320 meters. As before, these values are just barely in the limit accepted for the data set. This situation may explain why  $CT^2$  is smaller than it should be given the value of the intensity.

- Apart from this group of points, there are also two points ( $CT^2 = 0.6 \cdot 10^{-3}$ ,  $I = 465$ ) and ( $CT^2 = 10^{-3}$ ,  $I = 483$ ) which lie well below our fitted curve. These two consecutive points occur at 0450Z and 0556Z on 16 July. Before 0415Z there was a second and low

inversion layer, as stated earlier. After 0415Z, there is no apparent reason why there should be any cause to eliminate these two values. The disagreement may be due, as before, to non-stationarity, advection or unusual ambient noise which lead to stronger values of I compared to real value of  $CT^2$ . The next point, which ( $CT^2=2 \cdot 10^{-3}$ ,  $I=479$ ) was obtained at 0626Z is in much better agreement with the fitted curve.

d. Level 4

At this level, the zero of the curve seems to start at about  $I=350$ . There are still two points which appear to be out of range, ( $CT^2=0.6 \cdot 10^{-3}$ ,  $I=459$  and  $CT^2=0.96 \cdot 10^{-3}$ ,  $I=478$ ), probably for the same reasons suggested in the previous paragraph.

There are three different domains evident in this plot. The first represents the points with low values of  $CT^2$ , which are around a value of  $I=350$ . Some of these points have very low values of the backscattered signal which occurred during the first two days of the study period. There is a lot of scatter among the points in this area, probably because conditions were near neutral, with small values of  $T_a - T_s$  (difference between air temperature and surface temperature). So the relative effect of instrumental error on  $T_a - T_s$  may be very large. This scatter may also be due to the fact that, even for low values of  $CT^2$ , the system gives too-high values of I because of the background and system noise.

The second area contains the seven points around  $CT^2=0.5 \cdot 10^{-3}$  and  $I=400$ . They all correspond to the same period, from 0000Z to 0320Z on 16 July, and are described satisfactorily by a straight line segment. The third area includes points where  $CT^2 > 1.5 \cdot 10^{-3}$  and  $I > 460$ . Again, all of these points occur during the period from 0615Z to 2040Z on 16 July. In this case, the points may be described by a straight line from ( $CT^2=1.8 \cdot 10^{-3}$ ,  $I=470$ ) to ( $CT^2=4.5 \cdot 10^{-3}$ ,  $I=490$ ). Therefore, the overall set of points can be described by three different line

segments although the first one will not be very reliable because of scattering.

e. Level 5

Starting at this level, a lot of profiles whose inversion layer height is less than 380 meters must be rejected. These cases are essentially in area one where we got low values of  $CT^2$  in level 4. So little information is lost and most of the interesting profiles of level 4 are still there in that case.

It can be noted that the slope of the fit looks less curved than for previous levels.

f. Level 6.

This level gives results similar to level 5, although we do not have a well-defined straight line in the second area. But the general tendency remains the same and shows good agreement with the previous plots.

## 2. Calibration of the System

To obtain a reliable calibration curve, the plots that are likely to be free of reverberation effects will be kept. These correspond to the last three levels (4, 5 and 6). Here the points corresponding to the profiles taken at 0450Z and 0556Z on 16 July are eliminated for the reasons described earlier. The combination of these three plots is shown in figure 4.2.

The three sets of data superimpose quite well but do not fit on a straight line as expected if there is proportionality between  $CT^2$  and  $I$ . However, it is useful to plot the same data in logarithmic coordinates,  $\log(CT^2)$  versus  $\log(I)$ , to investigate whether a power relation provides a better fit for the relation between  $CT^2$  and  $I$ . The resulting plot is shown in figure 4.3. The two

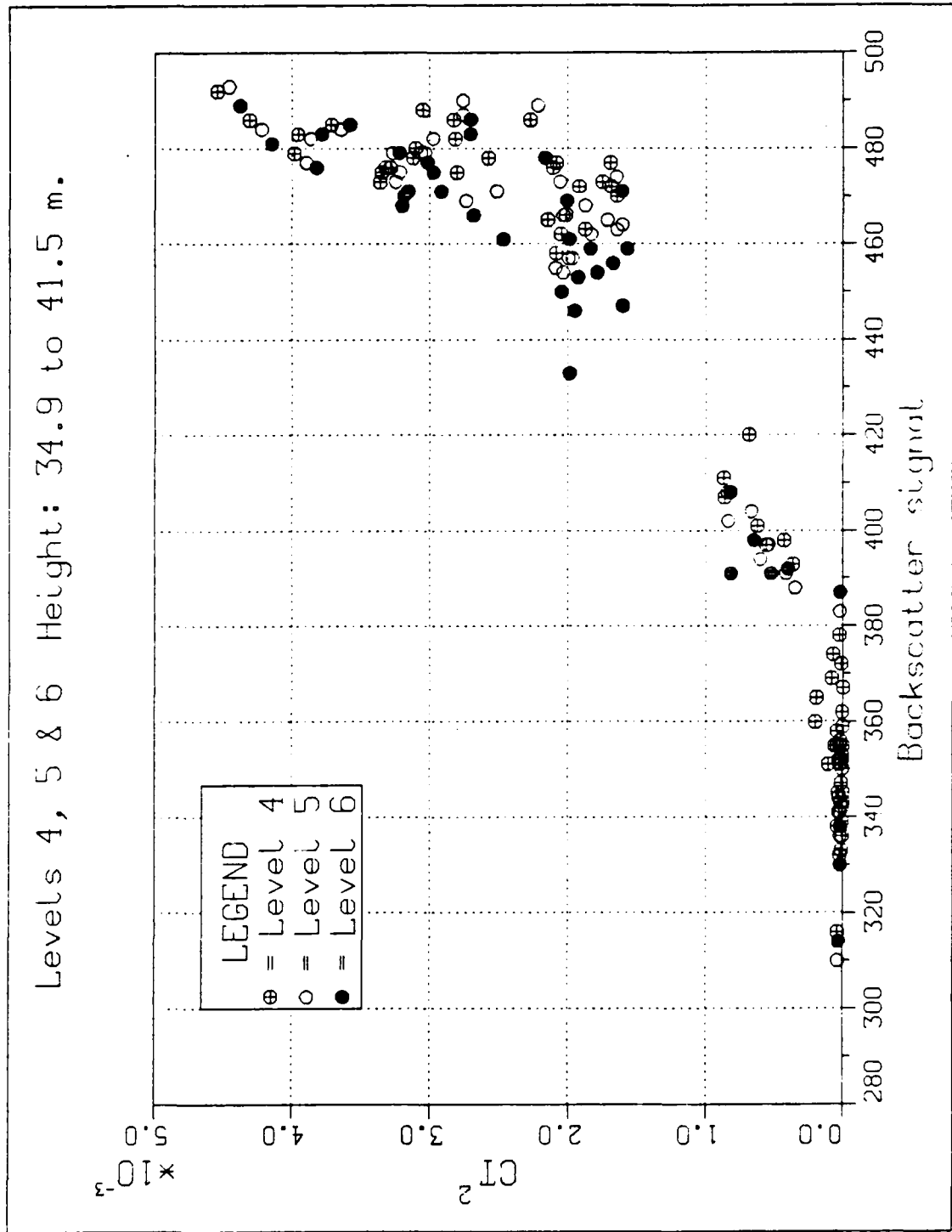


Figure 4.2  $CT^2$  versus Backscatter Intensity at Levels 4, 5 and 6.

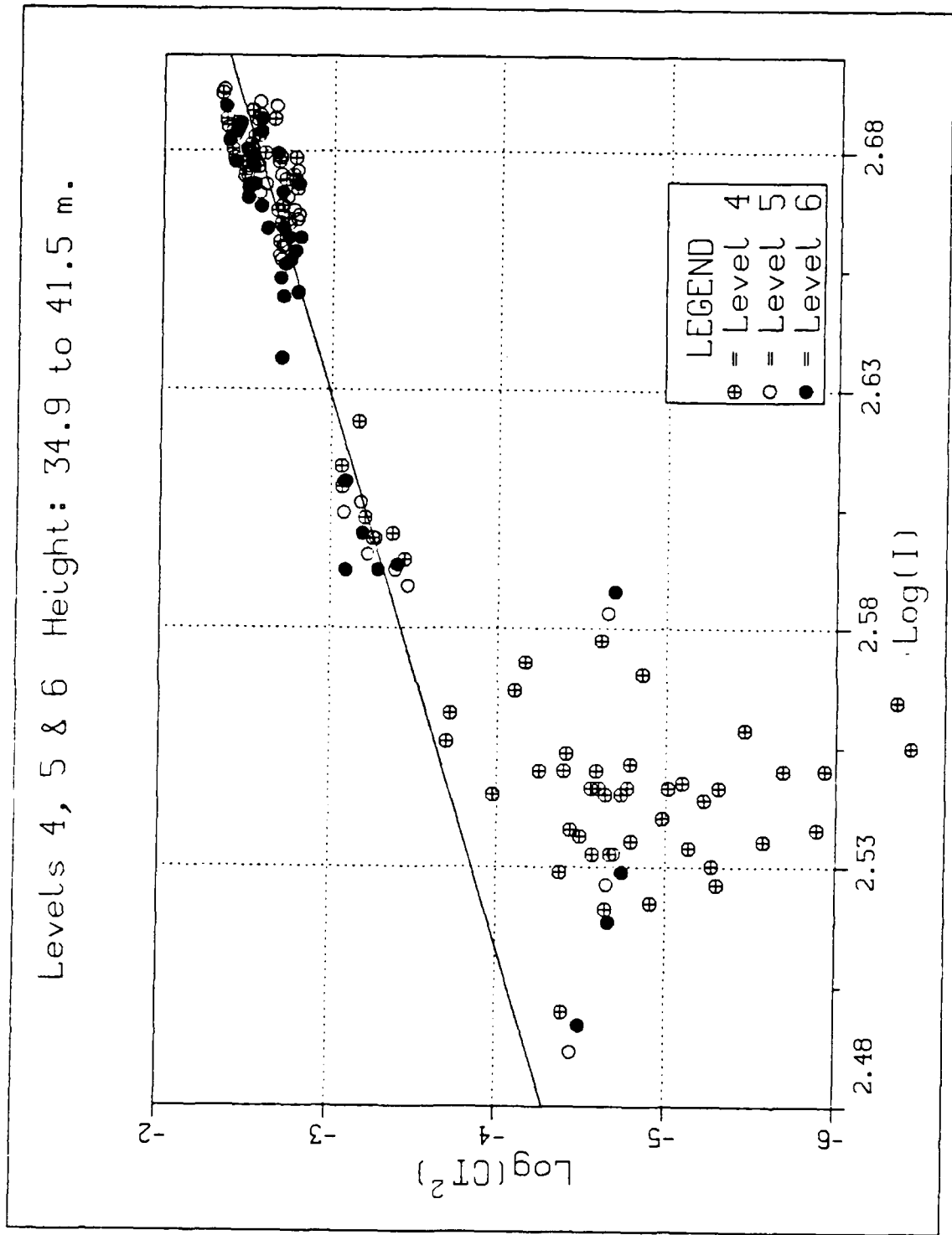


Figure 4.3  $\text{Log}(CT^2)$  versus  $\text{Log}(I)$  at Levels 4, 5 and 6.

regions with higher backscattered signal fit rather well on a straight line. The least-squares approximation gives the following equation:

$$\text{Log}(CT^2) = 8.63 \text{ Log}(I) - 25.66 \quad (4.1)$$

For lower values of I, there is much scatter in the data. This is more apparent on this figure. Therefore, the calibration given by equation 4.1 should be used carefully for I less than 380.

### 3. Error Analysis

To find the relative error on  $CT^2$  the value of the variance  $\sigma^2$  is first computed using the approximation:

$$\sigma^2 = 1/N \sum (\log(CT^2) - 8.63\log(I) + 25.66)^2$$

where N is the total number of points considered.  $\sigma^2$  is found to be equal to 0.01. The relative standard error on  $\log(CT^2)$  is given by:

$$d(\log(CT^2))/\log(CT^2) = \sigma^2/\log(CT^2)$$

whose left hand side is also equal to:

$$d(\ln(CT^2))/\ln(CT^2) = d(CT^2)/(CT^2 \ln(CT^2))$$

These expressions give:

$$d(CT^2)/CT^2 = \sigma^2 \ln(CT^2)/\log(CT^2)$$

Finally, the relative uncertainty on  $CT^2$  is:

$$d(CT^2)/CT^2 = \sigma^2 \log(10) = 23\%$$

### B. *TIME-HEIGHT CROSS-SECTIONS OF THE INVERSION LAYER*

There are several gaps in the time history of the sodar data, so the figures showing the boundary layer and its inversion obtained from sodar data are decomposed as follows:

Figure 4.4a : 11 July 2150Z to 12 July 1100Z.

Figure 4.4b : 13 July 0230Z to 2400Z.

Figure 4.4c : 14 July 0000Z to 2400Z.

Figure 4.4d : 15 July 0000Z to 2400Z.

Figure 4.4e : 16 July 0000Z to 2400Z.

Figure 4.4f : 17 July 0000Z to 1130Z.

The data are placed in a two dimensional array, one carrying the time, the other the altitude (or the gate). The lowest value of the backscatter intensity to be plotted is determined by a value "BSMIN". This is chosen for each plot such that the isopleths are so crowded, and the surface layer and the interfacial layer are most apparent. The lower the strength of the inversion layer, the lower the value of BSMIN. An incremental value is also chosen so that the contour lines are not too tightly spaced. The plot gives essentially a contour of the backscattered signal, but the values of  $CT^2$  according to the previous calibration have been added.

The resulting plots are first examined and their behavior are discussed as it relates to environmental conditions. Before doing this, it must be recalled that the summer "night" in these latitude is much like day. In fact, the downward radiation during the night is roughly equal to 2/3 of the value during daytime.

#### 1. 11 and 12 July

This period, which includes the night between days 11 and 12, shows a smooth and continuous decrease in the inversion layer. This is associated with a more stable layer which characterized the night time and a relatively high pressure (1013 mb) on 12 July between 1200Z and 2400Z which caused subsidence and tended to lower the inversion altitude. The low value of the chosen BSMIN (290) indicates that the strength of the inversion is not very great. The background noise for the period is about 230, not very far below 290.

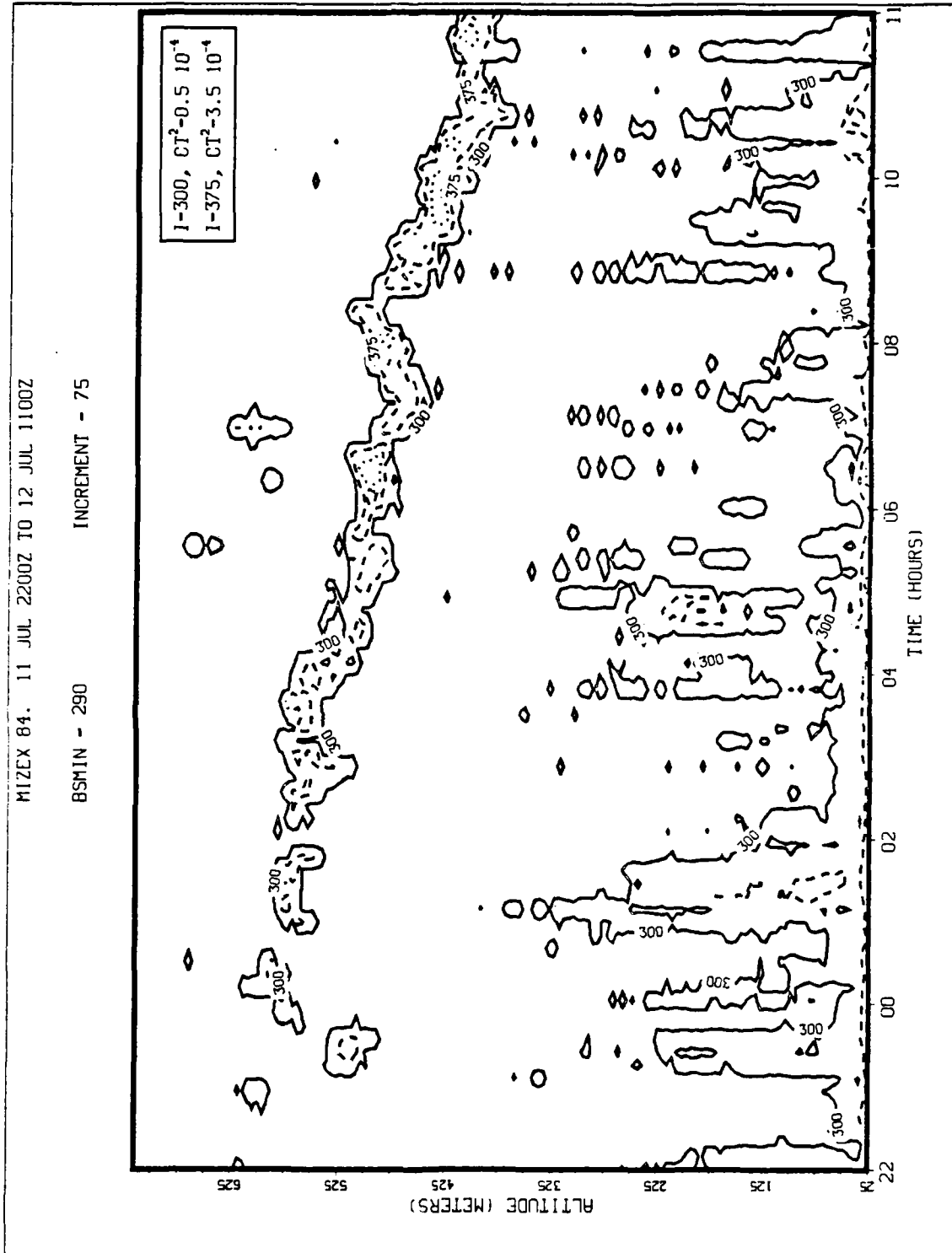


Figure 4.4a Atmospheric Boundary Layer Structure on 11 and 12 of July.

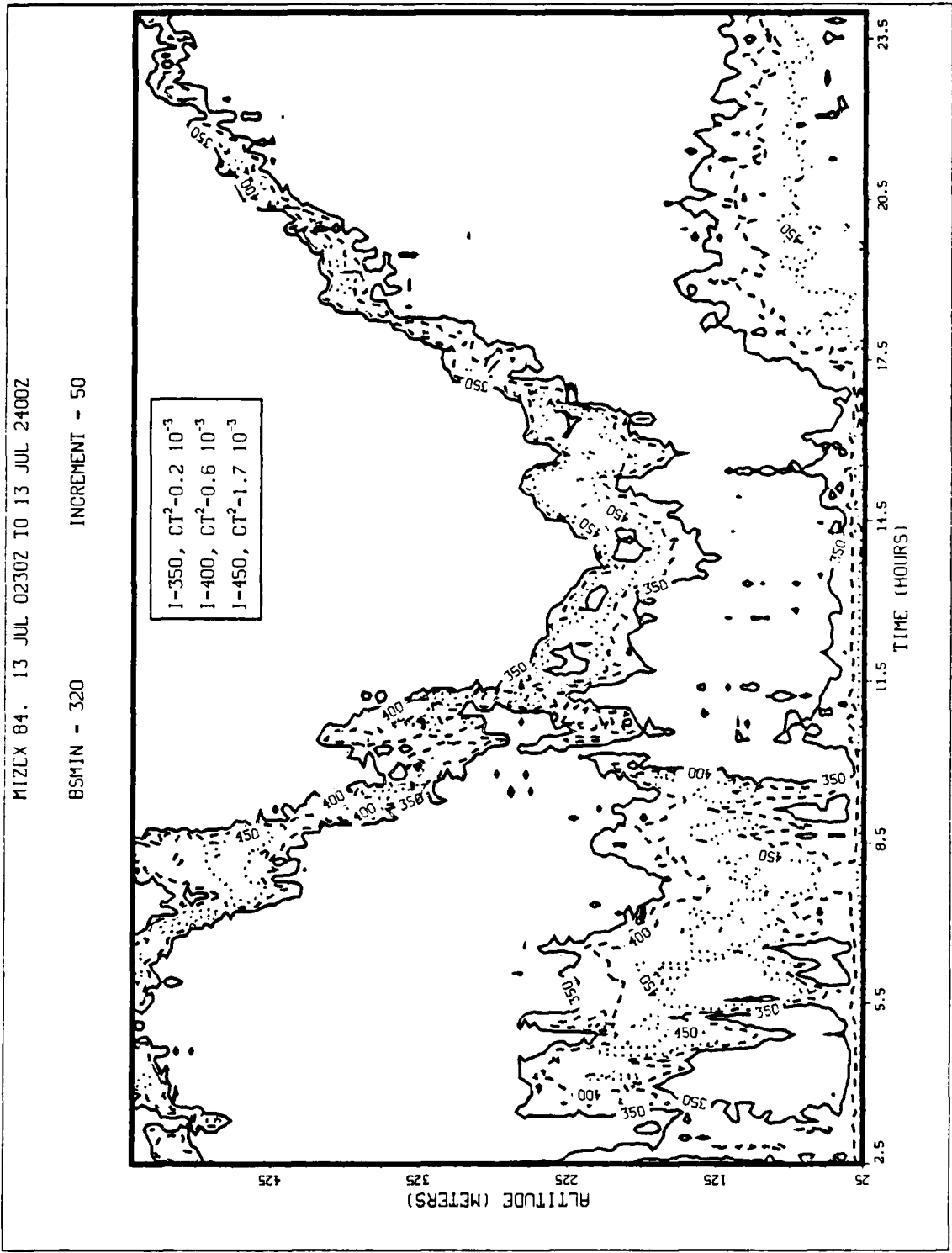


Figure 4.4b Atmospheric Boundary Layer Structure on 13 of July.

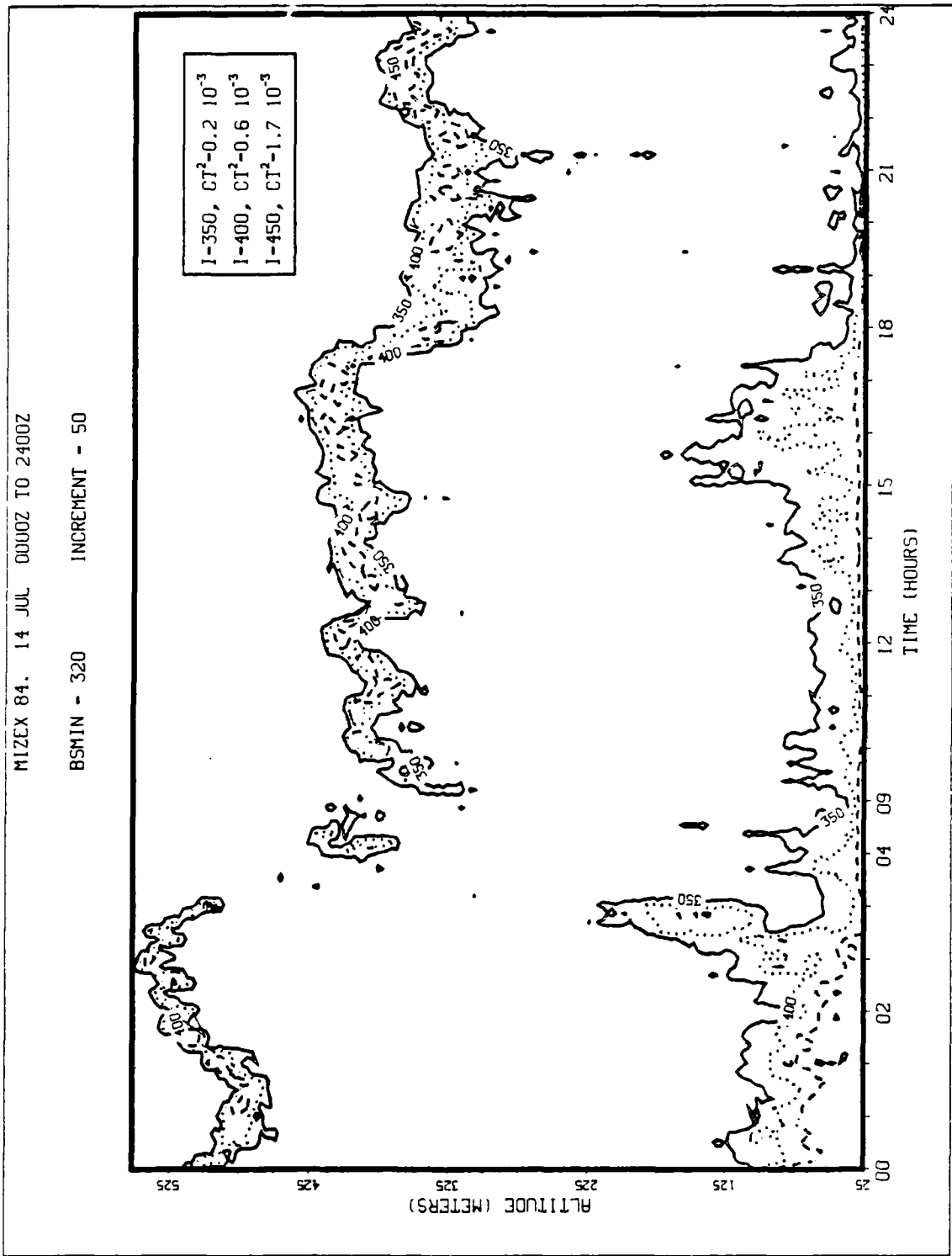


Figure 4.4c Atmospheric Boundary Layer Structure on 14 of July.

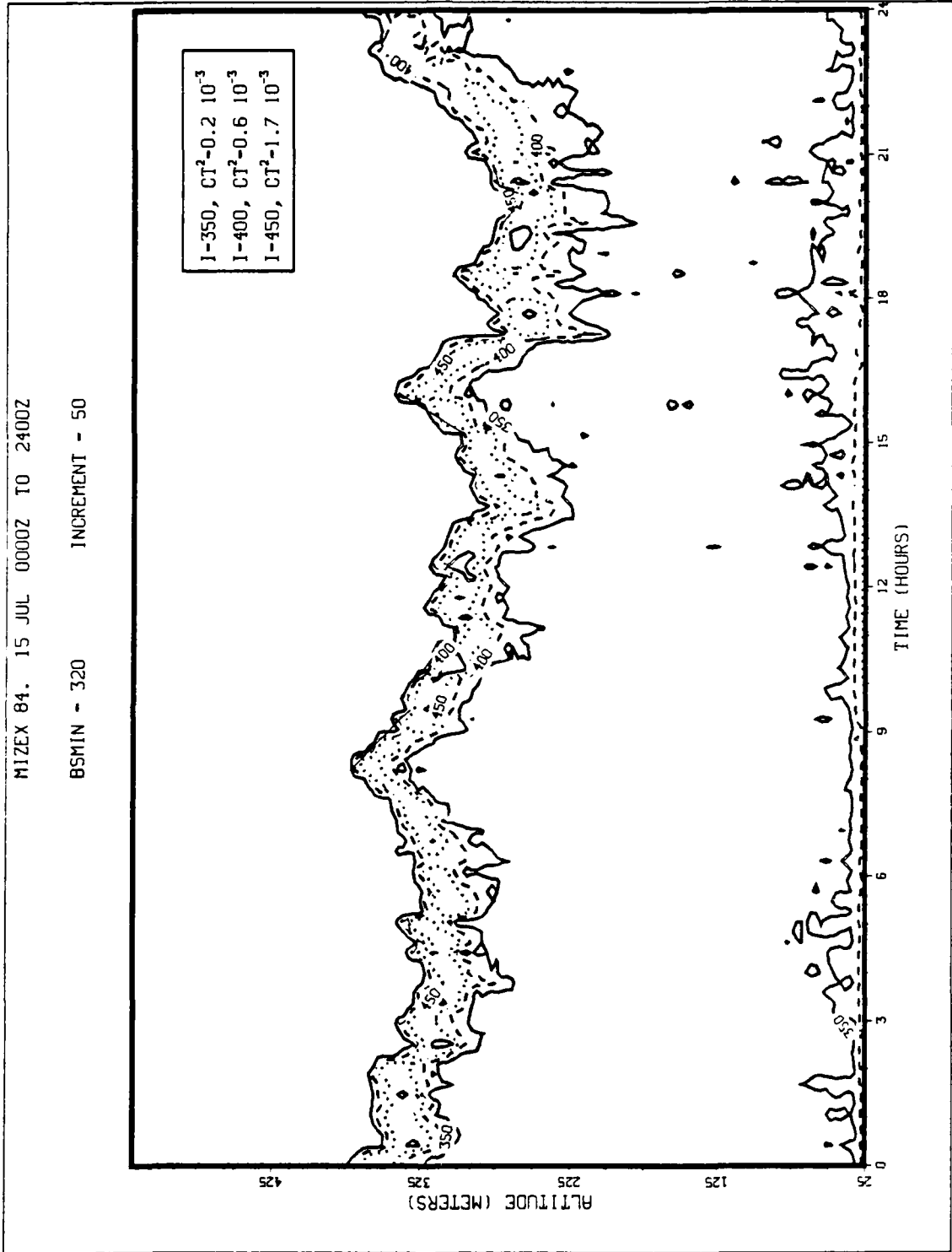


Figure 4.4d Atmospheric Boundary Layer Structure on 15 of July.

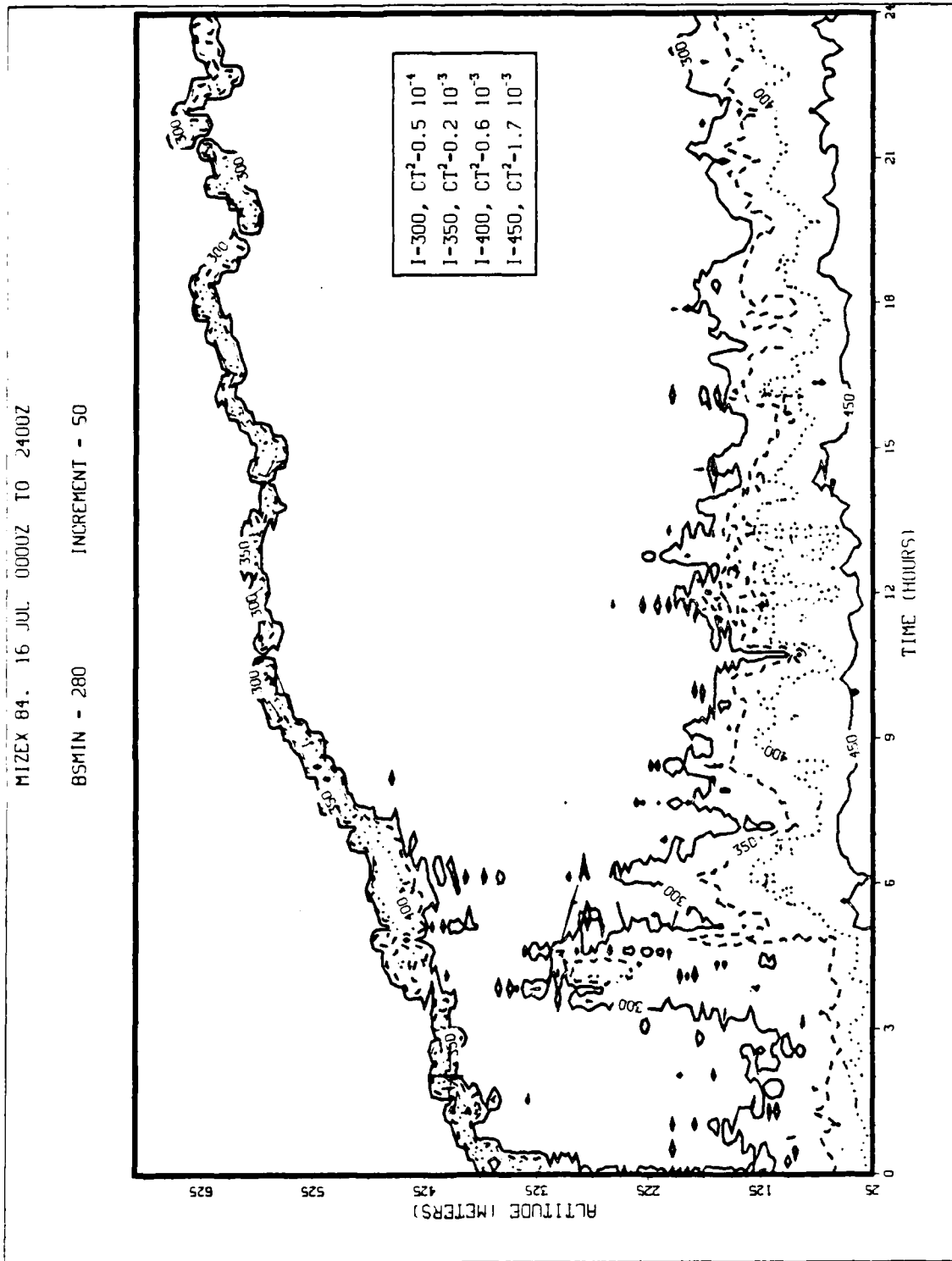


Figure 4.4e Atmospheric Boundary Layer Structure on 16 of July.

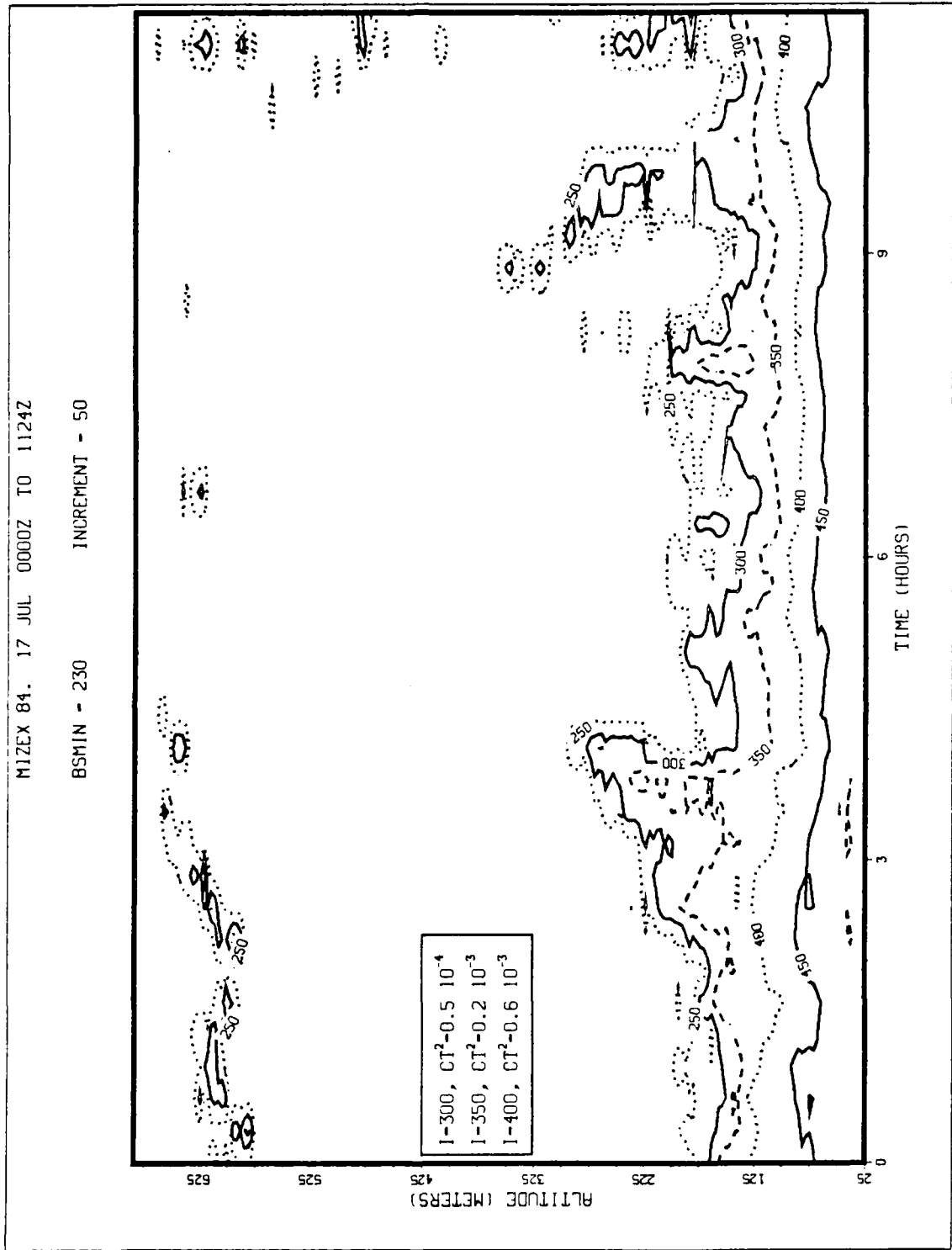


Figure 4.4f Atmospheric Boundary Layer Structure on 17 of July.

## 2. 13 July

In the second half of the night we see, as before, a decrease in the inversion layer. The stability which tends to occur contributes to the development of a period of intermittent strong backscatter at intermediate levels which rose and mixed with the higher one after sunrise.

Until noon, the wind speed was low and  $U^*$  was about 10 cm/s. Then  $U^*$  increased to 40 cm/s and remained between 30 and 40 cm/s until 1800Z. This indicates a stronger mechanical mixing, which raises the inversion layer through entrainment. Of course this increase may also occur as a response to the incoming solar radiation, which generated more unstable conditions and therefore buoyant mixing during the day.

Dorman (1985) suggests that gravity waves may contribute to the kind of movements of the inversion that we can see during this day. This, as well as advection, can cause the deepening and then the raising of the inversion layer. It is difficult here to have a quantitative appreciation of these effects because of the lack of supporting environmental data. A higher value of BSMIN (320) indicates the strength of the inversion layer for this day.

## 3. 14 July

There were no data between 0503Z and 0911Z. This caused a jump in the time scale for the plot of the inversion layer. This plot has been smoothed by the averaging process. In fact the true inversion height goes from 500 meters at 0500Z to 390 meters at 0900Z.

There was another gap between 2028Z and 2203Z, but the inversion stayed nearly at the same height during this interval. This is why the horizontal scale of figure 4.4c does not show an interruption for this short period.

As before, a stronger backscatter region developed at intermediate level from 0330Z until 0600Z. This is not easy to see

on the plot because of the lack of data, but in this case it rises up to 180 meters then disappears with the early morning. This may be caused by large-scale processes such as waves or advection. This day is also characterized by a weaker inversion layer.

#### 4. 15 July

There are no data for a one hour period between 1620Z and 1727Z. The inversion layer went from 265 meters to 245 meters, which is a decrease of less than 10%. Therefore there is no need for an interruption in the horizontal scale of figure 4.4e, although the reader should be aware of this gap period.

There was not much change during this 24 hour period. The signal in the inversion layer has a value greater than 450. This and the 13 July data were the two periods where the inversion layer will have probably the strongest temperature gradients.

#### 5. 16 July

The heat flux was negative (downward) during this entire day, and conditions were therefore stable. The temperature on the ice mast at 5.5 meters went from 0.2°C at 0000Z to 1°C at noon and up to 2°C at 2400Z. The temperature just above the ground was around 1°C from 1000Z to 1700Z and continued to increase to 1.7°C at 2400Z. These values of the ambient temperature were slightly higher than the other days.

This increase of the net heat in the boundary layer should be responsible for the continuous growth of the inversion layer during all the day. It is not easy to see what role the subsidence played because we were in a period of high pressure (1016 mb), with subsidence expected to lower the inversion layer height. Obviously, this was not the case here. The wind speed remained between 4 and 6 m/s until noon and then increased and stayed between 6 and 9 m/s. This wind caused more mechanical

mixing and may also be responsible for the increasing inversion layer height.

## 6. 17 July

The wind continued to be relatively strong during this day. It stayed between 7 and 10 m/s and is probably the reason why the inversion layer continues to behave as it did during the day before. There are no *in situ* data of  $U^*$  and  $T^*$  for this period to get the value of the heat flux. The temperature just above the ice and at 5.5 meters are very close, so conditions must have been near-neutral. This can explain the weak inversion layer which tends to vanish and the greater interval in the surface layer between the contour lines than on the previous days. This was a time of formation of an area of stronger backscattered signals at intermediate levels around 03-0400Z and 0900Z, which decayed subsequently.

### C. ESTIMATION OF POTENTIAL TEMPERATURE JUMP AND REFRACTIVE-INDEX GRADIENT AT THE INVERSION LAYER

#### 1. The Potential Temperature Jump

Wyngaard and Lemone (1980) derived an equation which shows that it is possible to relate the mean value of the virtual temperature structure parameter with the jump of potential virtual temperature at the inversion layer, the height of the inversion and the virtual temperature scaling parameter:

$$\langle CT_v^2 \rangle = 0.5 T_v^* \Delta T_v / Z_i^{2/3} \quad (4.2)$$

where the brackets mean average over the inversion layer and the subscript  $v$  indicates virtual temperature. This is only valid for convective cases. However, since there were no strong free

convection conditions in the Arctic, we will consider unstable cases for values of  $Q_0$  greater than  $10^{-3}$  °K m/s.

Wyngaard and Lemone also show how to estimate the potential temperature jump at the inversion, assuming that the surface moisture flux and the mean humidity jump can be neglected at the top. These assumptions allow use of normal temperature instead of virtual temperature.

$$T_{v^*} = T^*$$

$$T_v = T$$

The first assumption is reasonable because  $q^*$  is very small in this experiment, so the vapor flux  $U^*q^*$  will be negligible. The second assumption is not so reasonable because the value of the humidity jump at the inversion is not known. The presence of fog in the area is an indicator of moisture, but it can be expected that the cold temperatures (0°C) will produce a generally drier atmosphere (due to lower saturation vapor pressure). Radiosonde data will be helpful in that case but are not currently available. Therefore, the deduction of the inversion layer potential temperature jump should be taken as a first guess. With these qualifications, equation 4.2 can be rewritten:

$$\Delta T = 2 \langle CT^2 \rangle Z_i^{2/3} / T^* \quad (4.3)$$

The only problem now is to compute the mean of  $CT^2$  in the inversion layer. Wyngaard and Lemone recommend assuming a peak-to-mean ratio for  $CT^2$  of 2. The peak value for  $CT^2$  is easily determined because we know  $Z_i$  and the corresponding value of the backscatter signal. Then equation 4.1 is used to get the value of  $CT^2$  at the peak ( $CT_p^2$ ), which allows to infer the potential temperature jump in the inversion. Equation 4.3 becomes:

$$\Delta T = CT_p^2 Z_i^{2/3} / T^* \quad (4.4)$$

## 2. Refractive Index Gradient at the Inversion Layer

### a. Derivation of the Refractive Index Gradient

The value of the refractive index gradient at the inversion layer can be obtained from the equation for refractivity (Meeks, 1982):

$$N = 77.6 P/T + 3.73 \cdot 10^5 e/T^2 \quad (4.5)$$

Where  $P$  and  $e$  are the atmospheric pressure and the water vapor pressure respectively in millibars and  $T$  is the temperature in  $^{\circ}\text{K}$ . Assuming that  $e$  is negligible which is compatible with the previous assumption to derive  $\Delta T$ , and taking the derivative with respect to  $Z$ , equation 4.5 becomes:

$$dN / dZ = m + n dT/dZ \quad (4.6)$$

Where:

$$m = (77.6/T) dP/dZ$$

$$n = -77.6/T^2$$

$P$  at the surface was approximately equal to 1005 mb. The ratio  $dP/dZ$  is given by the hydrostatic approximation:

$$dP/dZ = - Pg/RT \quad (4.7)$$

where  $R$  is the gas constant. For normal atmospheric conditions  $R = 287 \text{ J}^{\circ}\text{K}^{-1}\text{kg}^{-1}$ . Assuming that  $T = 273^{\circ}\text{K}$ , we get  $dP/dZ = -125 \text{ mb/km}$ . The inversion height was typically 400 meters, which gives  $P = 960 \text{ mb}$  at the inversion and the new value of  $dP/dZ$  in the inversion layer reduces to  $-120 \text{ mb/km}$ .

Then the values of the two parameters  $m$  and  $n$  are:

$$m = -34 \text{ km}^{-1}$$

$$n = -0.001 \text{ }^{\circ}\text{K}^{-1}$$

Equations 3.16, 4.4 and 4.6 give the value of  $dN/dZ$  at the inversion:

$$dN/dZ = -34 - (CTp^2 Z_i^{2/3} / T^* Th) \quad (4.8)$$

Where  $Z_i$  and  $Th$  are in meters and  $dN/dZ$  in  $km^{-1}$ .

#### b. Refractive Index Gradient and Refraction

Hitney *et al.* (1981) developed the Integrated Refractive Effects Prediction System (IREPS), which is used to determine the radar coverage in an area as a function of the refractive condition determined by atmospheric parameters as pressure temperature and humidity. IREPS classification defines the following conditions of refraction with respect to  $dN/dZ$ :

Subrefraction:	$0 < dN/dZ$
Normal:	$-79 < dN/dZ < 0$
Super refraction:	$-157 < dN/dZ < -79$
Trapping:	$dN/dZ < -157$

The modified index of refraction  $M$  is related to  $N$  by the formula:

$$M = N + 157 Z \quad (4.9)$$

Where  $Z$  is the height in km. Therefore we will have trapping when  $dM/dZ < 0$  or  $\Delta M < 0$  for a positive  $dZ$ .

#### c. Computed Refractive Conditions

The values of  $\Delta T$ ,  $dN/dZ$ ,  $\Delta M$  and some variables used to retrieved these values are given in appendix "B". figure 4.5 show the profile of  $\Delta M$  versus time in the inversion layer. The trapping conditions happen for the points which are below the horizontal line ( $\Delta M=0$ ). Some particular points have been emphasized by

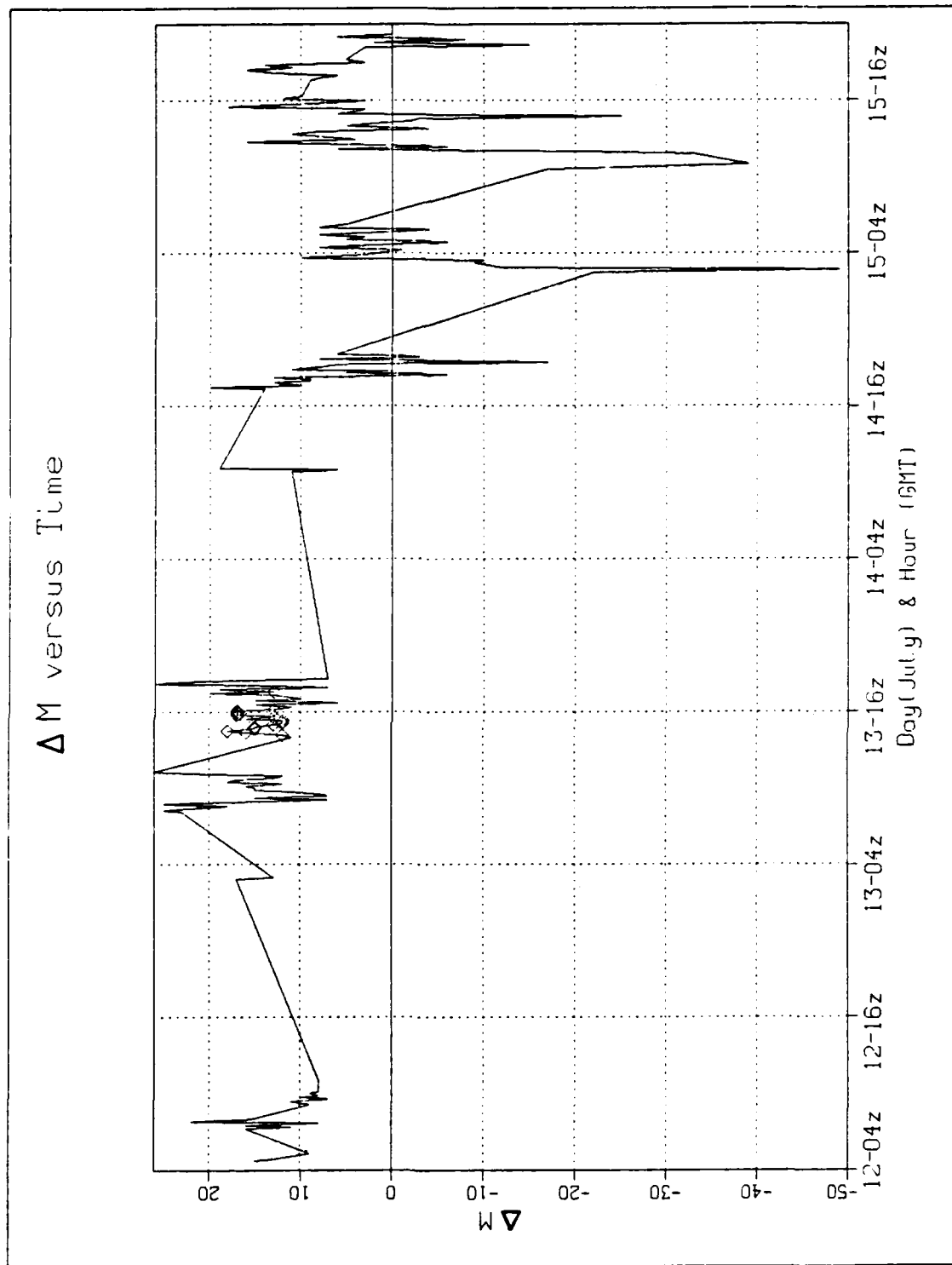


Figure 4.5  $\Delta M$  versus Time in the Inversion Layer.

a marker. They depicted the largest 10 % of  $Q_0$  values. Under these conditions, the computation should be more accurate because these values are closest to the free convection case.

The refraction is generally normal until 1800Z on 14 July. After this period and until 2200Z on 15 July there are much stronger values for  $dN/dZ$  as well as for  $\Delta T$ . But there are some important fluctuations in the range of this data and the values obtained for  $\Delta T$  look sometimes very high for the corresponding thickness of the layer which stays between 80 and 150 meters. These fluctuations may be due to the different errors and approximations introduced in the computation. The more sensitive errors are recalled: error on  $Z_l$  and  $Z_u$  which determine the thickness, error on calibration of the sodar system which is use to get  $CT_p^2$  and approximation concerning the mean humidity jump at the inversion and the 1/2 factor to retrieve the mean value of  $CT^2$  from its peak value in the inversion layer. The major error is probably the free convection assumption. The highest values of  $\Delta T$  occurred very often when  $Q_0$  is smallest, which means that the situation is less unstable and that equation 4.4 is probably not valid, which is not surprising. All these features indicate caution is required in interpreting these results. However, it is possible to deduce some general tendencies during the covered period. There should be more refractive conditions during 15 July with some peaks around 0200Z and between 1000Z and 1100Z. This stronger refraction was expected in section "B.4" when looking at the time-height cross-section, because of the stronger values of the backscattered signal in the inversion layer. On the other hand the same expected result is not obtained for the 13 July, which shows only two periods (1642Z and 1702Z) with  $dN/dZ$  smaller than  $-79 \text{ km}^{-1}$ .

The restriction concerning the validity of the computation for unstable cases only, does not allow to have any data after 15 July at 2200Z, because then  $Q_0$  becomes too small.

### 3. Comparison of some Results with Radiosonde Data

At the time this thesis was written, there were only two radiosonde profiles available. They are showed in figure 4.6 and were taken from 13 July at 1100z and 14 July at 1103Z. The left profiles represent temperature and dew point with respect to height whereas the right profiles depict the wind speed and direction.

#### a. Comparison with Radiosonde of 13 July at 1100Z

The upper and lower levels of the inversion measured on figure 4.6 give respectively 370 and 240 meters, which result in a thickness of 130 meters. The corresponding  $\Delta T$  is equal to  $3.5^{\circ}\text{K}$ . The program which computes  $Z_u$  and  $Z_l$  gave us 366 and 273 meters at 1057Z and 369 and 204 meters at 1107Z, respectively. Therefore, the two values of the upper level are in very good agreement. For the lower level and after an extrapolation between 1057Z and 1107Z to find the value at 1100Z (about 1/3 of the interval), a value of 230 meters is found which is also in good agreement with the radiosonde data.

The values of  $\Delta T$  have been obtain with equation 4.4 by reading directly the values of  $T^*$  from the *in situ* data set and the values of  $I$  and  $Z_i$  for the other data set. Each of these are averaged about every 10 minutes. It is assumed that there is coincidence when the time between the two data sets is less than 5 minutes. The value of  $\Delta T$  from 1047Z to 1117Z are: 3.4, 2.8, 5.6, 2.6, the closest being equal to 2.8 at 1057Z. This is fairly good agreement with the  $3.5^{\circ}\text{K}$  given by the radiosonde.

#### b. Comparison with Radiosonde of 14 July at 1103Z

Proceeding as before, we look at the set of values surrounding 1103Z. The first one is at 1100Z ( $Z_u= 382$  m,  $Z_l= 336$  m) and the other one at 1107Z ( $Z_u= 382$  m,  $Z_l= 253$  m). This gives at 1103Z: 382 m for the upper level and 300 m for the lower. The radiosonde

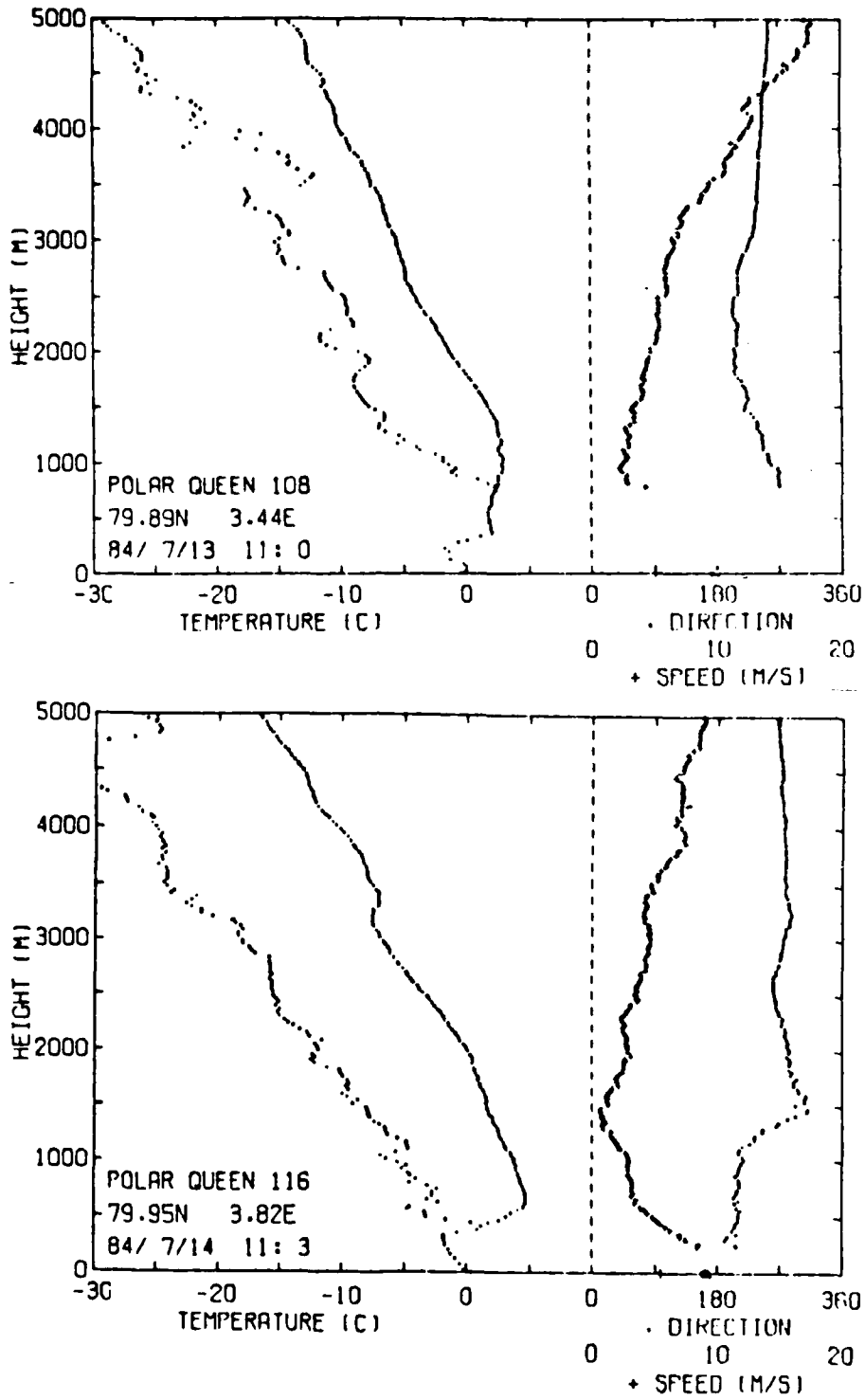


Figure 4.6 Radiosonde Measurements for Two Different Times.



measurement gives respectively 510 and 320 meters. The base of the inversion seems to be correct, but at the top there is a big difference. A reason which can explain this discrepancy may be found on the display terminal whose shaded plot is reproduced in figure 4.7. after 1100Z, just above the marked dark inversion layer, another shaded area can be seen which may be a weak prolongation of the inversion layer. This is probably too weak to be detected by the program, although the radiosonde responded to it. Also, the decay of turbulence above  $Z_i$  may be an explanation of this feature. This less turbulent part is associated with a weaker gradient of potential temperature than is the more turbulent part around  $Z_i$ . Of course, this will disturb the computation of  $\Delta T$  and  $dN/dZ$ . In fact, the radiosonde gives a value of  $9.1^\circ\text{K}$  while the program gives  $3.3^\circ\text{K}$  at 1053Z,  $1.4^\circ\text{K}$  at 1100Z and 1107Z which are out of range of the measured value.

Two comparisons are not enough to verify the method, but as the occurrence of the extended weak inversion layer is not common in the data set, we can expect to have a good agreement between the computed variables and the radiosonde data in most cases if we are in free convection conditions.

## V. CONCLUSIONS AND RECOMMENDATIONS.

The analysis of one particular week's data during the last days of MIZEX 84 was made for its well-formed inversion layer. This analysis allowed finding a power law to calibrate the sodar system which was used to study the atmospheric boundary layer. The method gives only two periods where the pairs of values  $CT^2$  and  $I$  were reliable for this calibration. Both are during 16 July, from 0000Z to 0300Z and from 0615Z to 2040Z. In the other cases, either there were no *in situ* data, or the inversion layer was too low, or we had formation of a second low inversion layer which does not allow use of the usual formulas to compute  $CT^2$  in the surface layer. It will be interesting in subsequent analyses to extend the method to other days of the experiment in order to see if the calibration remains in agreement with the relation found in this study.

This calibration does not seem to hold for values of  $I$  lower than 380 (or  $CT^2 = 4 \cdot 10^{-4}$ ). However, this is a minor problem because the values of  $CT^2$  in the inversion layer where the back-scattered signal has a value generally higher than 400, were mainly used in this study.

The time-height cross-sections give reliable pictures of the boundary layer and especially of the inversion layer. The numerical indications provide some complementary quantitative information on the value of the temperature structure parameter in the inversion layer.

The calibration relation was then used to deduce values of  $CT^2$  to estimate the potential temperature jump and the refractive index gradient in the inversion layer. The error is of order 23 %. Free convection formulations indicate that there should be trapping conditions on 15 July around 0200Z and 10-1100Z. However, since the computations are valid only for free convection, these results must

be considered with caution because  $Q_0$  was never very large, about  $10^{-3}$  °K/(m/s) for the trapping condition period. The highest value of  $Q_0$  was around  $2 \cdot 10^{-2}$  °K/(m/s) on 13 July between 1400Z and 1500Z, but the refractive index gradient indicated a normal propagation condition in the inversion.

The strength of the backscattered signal in the inversion should have lead to a trapping condition, especially on the 13th and 15th of July, according to the time-height cross-sections. This was confirmed for the 15 July, with the computation of the refractive index gradient. It was apparently not true on 13 July, although  $Q_0$  was higher on that day but probably not high enough to be a free convection case as required by the theory.

The comparison of free convection-determined  $\Delta T$ 's with some radiosonde data was quite good in one case and erroneous in the other because of an higher inversion layer top than expected from sodar data. To make a better comparative analysis, it will be necessary to obtain more radiosonde data. This should be a productive avenue for future analysis.

Another source of error of which we were aware too late to consider was that the value of  $I$  given by the sodar data is in fact the summation of the backscattered power and a spreading loss correction term  $\Delta I$  which is equal to:

$$\Delta I = \ln(t/4)^2 - 50$$

where  $t$  is the tir in ms for a pulse to propagate from the antenna to the middle of a gate. Therefore  $\Delta I$  is a function of altitude and goes from -44 (for  $z = 25m$ ) to about -38 when  $z = 500m$ . This represents approximately a 10 % error in the surface and in the inversion layer. This should not cause a significant change in the overall results, although it should be incorporated into further studies using this sodar system.

This kind of sodar study could be extended to other areas with stronger inversions and surface heat fluxes and could be a good means, even for an isolated platform, to detect ducting conditions when a radiosonde is not available.



```

1          'SIGNAL ZLOW|SIGNAL ZUP|          |'/1X,58('-'))
CCCCC
      *** There are two tapes to read in MSS
      *** UNIT 16: 11 12 July, FLAG = 1
      *** UNIT 11: 13 TO 17 July, FLAG = 2
      -----
      FLAG = 1
111     DO 42 L= 1, 2222
          DO 13 I= 1, NGATE
              IF (FLAG.EQ.2) GO TO 112
              READ (16,10,END=998)(INT(I,J),J=1, 256 )
              GO TO 13
112     READ (11,10,END=999)(INT(I,J),J=1, 256 )
10      FORMAT ( 2(128I5) )
13      CONTINUE

CCCCC
      *** We need to make some adjustments to the first
      *** level to consider to avoid the confusion with
      *** the surface layer. The number below are chosen
      *** after some run and looking at the display
      *** terminal for each period.
      -----
107     IF (FLAG.EQ.1) GO TO 113
          IF (INT(4,4).EQ.13.AND.INT(4,5).GT.10) IFL= 40
          IF (INT(4,4).GE.13.AND.INT(4,5).GT.21) IFL= 70
          IF (INT(4,4).EQ.14.AND.INT(4,5).GE.10) IFL= 80
          IF (INT(4,4).GE.15) IFL = 60
          IF (INT(4,4).GE.16) IFL = 110
          IF (INT(4,4).GE.16.AND.INT(4,5).EQ.5) IFL= 135
          IF (INT(4,4).EQ.17.AND.INT(4,5).GT.5) IFL= 120
      -----
CCCCC
      *** Make the average (BAC) of the signal (INT)
      =====
      -----
113     DO 38 J = 1,NVERT
          TOT = 0.0
          N = 0
          DO 22 I=1, NGATE
              K= J + IFL - 1

CCCCC
      *** Disregard too big values in the averaging process
      *** "K" means we compute average for the "Kth" level.
      -----
          IF (INT(I,K).GT.700) GO TO 22
          N = N + 1
          TOT= TOT + FLOAT( INT(I,K) )
22     CONTINUE

CCCCC
          IF (N.NE.0) GO TO 31
          BAC(K) = OUT
          GO TO 38
31     BAC(K) = TOT / FLOAT(N)
38     CONTINUE
      -----
CCCCC
      *** Compute " ZI "
      =====
      -----
41     DO 41 JK = 1, 280
          ZL1(JK) = 0.0
          BMAR(JK) = 0.0
          CONTINUE
          BMIN = BBB
          BMOU = 500.
          ZL = 0.

```

```

NNVERT = NVERT - 4
  IF (FLAG.EQ.1) DD = 7.
  IF (FLAG.EQ.2) DD = 5.
DO 55 I = 1, NNVERT
  BIBI = BBB
  AVG = 0.
  N = 0

```

CCCC

\*\*\* Average signal over "NZ" levels.

```

DO 50 J = 1, NZ
  K= IFL + J + I - 2
  IF (BAC(K).EQ.OUT ) GO TO 50
  IF (BAC(K).GE.BIBI) BIBI = BAC(K)
  N = N + 1
  AVG= AVG + BAC(K)
CONTINUE

```

50 C

```

IF (N.EQ.0) GO TO 55
BRUIT= AVG/FLOAT(N)

```

CCCC

\*\*\* ZI is chosen at the intermediate of the five  
 \*\*\* levels where the average signal is stronger.

```

IF (BRUIT.LT.BMIN) GO TO 52
ZI=25.+(DD*4./2./1000.*V) * FLOAT((I+1)+(IFL-14))
LEVEL = IFL + I - 12
BMIN = BRUIT
BMAX = BIBI
MAI = I

```

CCCC

\*\*\* Look for the lowest value of the signal  
 \*\*\* corresponding to a height "ZL1" to determine the  
 \*\*\* lowest boundary "ZL" of the inversion layer.

52

```

IF (BRUIT.GT.BMOU) GO TO 55
BMOU = BRUIT
BMAR(I) = BRUIT
ZL1(I)= 25.+(DD*4./2./1000.*V)*FLOAT((I+1)+(IFL-14))
CONTINUE

```

55

CCCC

\*\*\* Select the value "ZL" of "ZL1" which is below  
 \*\*\* ZI but above 25 meters which is the first level.

62

```

DO 62 II= 1, 280
  IF (ZL1(II).GE.ZI.OR.ZL1(II).LE.25.) GO TO 62
  ZL = ZL1(II)
  SIG = BMAR(II)
CONTINUE
IF (BMIN.LE.BBB) GO TO 42

```

CCCC

\*\*\* Compute the upper height of the inversion layer

```

IF (ZI.EQ.OUT ) GO TO 42
BLIM = BMIN / 2.
DO 75 II = MAI, NVERT
  AVG = 0.
  NN = 0
  DO 70 JJ = 1, NZ
    KK= IFL + JJ + II - 2
    IF (BAC(KK).EQ.OUT ) GO TO 70
    NN = NN + 1
    AVG= AVG + BAC(KK)
  CONTINUE
  IF (NN.EQ.0) GO TO 75

```

70

```

BRUIT = AVG / FLOAT (NN)
IF (BRUIT.LT.BLIM) GO TO 77
SIGU = BRUIT
ZU=25.+(DD*4./2./1000.*V)*FLOAT((II+1)+(IFL-14))
75 CONTINUE
C C C C C
** Estimate the thickness of the inversion layer
-----
77 THI = ZU - ZL
C C C C C
** Write date, time, average max. backscatter
** signal, ZI, SIG, ZL, SIGU, ZU, THI.
-----
WRITE( 6, 35) (INT(4, I), I=4, 6), BMIN, BMAX, ZI, SIG, ZL,
* SIGU, ZU, THI
WRITE(15, 35) (INT(4, I), I=4, 6), BMIN, BMAX, ZI, SIG, ZL,
* SIGU, ZU, THI
35 FORMAT (1X, '|', I2, 'JUL', 1X, I2, 'H', I2, '|',
1 F4.0, 1X, F4.0, 1X, F4.0, 'M', '|', F4.0, '|', F4.0, 'M', '|',
2 F4.0, '|', F4.0, 'M', '|', F4.0, 'M', '|')
42 CONTINUE
998 IF (FLAG.EQ.2) GO TO 999
FLAG = 2
GO TO 111
999 WRITE (6, 456)
456 FORMAT ( 1X, 58 ('-'))
STOP
END

/*
//GO.FT11F001 DD DSN=MSS.S0985.MIZE20,MSVGP=PUB4C,
DCB=(RECFM=FB,LRECL=1280,BLKSIZE=6400),
UNIT=3330V,DISP=(OLD,KEEP)
//GO.FT16F001 DD DSN=MSS.S0985.MIZE13,MSVGP=PUB4C,
DCB=(RECFM=FB,LRECL=1280,BLKSIZE=6400),
UNIT=3330V,DISP=(OLD,KEEP)
//GO.FT15F001 DD DSN=MSS.S0985.ZIBB7,MSVGP=PUB4C,
DCB=(RECFM=FB,LRECL=1280,BLKSIZE=6400),
UNIT=3330V,DISP=(NEW,CATLG)
//

```

APPENDIX B  
TABLE OF ZI, QO, T\*, DN/DZ AND ΔM

Date	Time	Zi	Th	CT <sup>2</sup>	Qo	T*	Δ T	dN/dZ	Δ M
12 Jul	446Z	493.	102.	0.0011	0.0019	-0.097	0.7	-7.	15.
12 Jul	454Z	488.	88.	0.0011	0.0026	-0.060	1.2	-13.	13.
12 Jul	521Z	502.	60.	0.0006	0.0047	-0.081	0.4	-7.	9.
12 Jul	715Z	474.	134.	0.0016	0.0014	-0.019	5.1	-38.	16.
12 Jul	723Z	484.	125.	0.0031	0.0012	-0.022	8.8	-71.	11.
12 Jul	731Z	493.	120.	0.0008	0.0016	-0.020	2.6	-22.	16.
12 Jul	741Z	502.	74.	0.0017	0.0014	-0.027	0.0	-55.	8.
12 Jul	749Z	488.	144.	0.0002	0.0014	-0.027	0.5	-4.	22.
12 Jul	758Z	470.	116.	0.0008	0.0020	-0.025	1.9	-16.	16.
12 Jul	87Z	470.	97.	0.0005	0.0015	-0.050	0.6	-7.	15.
12 Jul	88Z	428.	70.	0.0025	0.0038	-0.068	2.1	-30.	9.
12 Jul	917Z	433.	79.	0.0015	0.0027	-0.037	2.3	-29.	10.
12 Jul	926Z	424.	79.	0.0012	0.0028	-0.038	1.3	-22.	11.
12 Jul	935Z	419.	65.	0.0029	0.0025	-0.053	0.0	-47.	17.
12 Jul	943Z	405.	74.	0.0015	0.0033	-0.062	1.1	-18.	10.
12 Jul	952Z	386.	56.	0.0011	0.0053	-0.111	0.0	-9.	8.
12 Jul	102Z	391.	60.	0.0017	0.0048	-0.112	0.0	-14.	9.
12 Jul	1010Z	400.	51.	0.0008	0.0048	-0.112	0.0	-14.	9.
12 Jul	112Z	396.	56.	0.0029	0.0067	-0.299	0.0	-9.	8.
13 Jul	1249Z	492.	132.	0.0014	0.0016	-0.027	3.3	-25.	17.
13 Jul	258Z	492.	132.	0.0013	0.0011	-0.038	2.6	-22.	13.
13 Jul	887Z	449.	189.	0.0024	0.0013	-0.022	6.3	-33.	23.
13 Jul	8816Z	449.	195.	0.0023	0.0013	-0.022	6.6	-31.	25.
13 Jul	8834Z	432.	169.	0.0024	0.0012	-0.016	8.8	-52.	18.
13 Jul	8845Z	406.	202.	0.0016	0.0010	-0.012	7.7	-35.	25.
13 Jul	993Z	373.	109.	0.0024	0.0013	-0.012	10.2	-94.	7.
13 Jul	9912Z	353.	136.	0.0017	0.0011	-0.013	6.6	-49.	15.
13 Jul	9923Z	339.	96.	0.0032	0.0017	-0.018	6.6	-88.	7.
13 Jul	9932Z	326.	96.	0.0022	0.0016	-0.016	6.6	-69.	8.
13 Jul	9941Z	320.	106.	0.0016	0.0014	-0.014	5.5	-52.	11.
13 Jul	9951Z	313.	122.	0.0015	0.0021	-0.019	3.3	-31.	15.
13 Jul	1011Z	310.	116.	0.0018	0.0025	-0.025	3.3	-27.	15.
13 Jul	1010Z	300.	119.	0.0016	0.0032	-0.032	2.2	-19.	16.
13 Jul	1019Z	356.	96.	0.0019	0.0040	-0.033	2.2	-29.	12.
13 Jul	1029Z	316.	132.	0.0018	0.0048	-0.032	2.6	-20.	18.
13 Jul	1038Z	293.	122.	0.0020	0.0043	-0.033	2.6	-21.	17.
13 Jul	1048Z	326.	106.	0.0020	0.0051	-0.028	3.4	-32.	13.
13 Jul	1057Z	326.	93.	0.0017	0.0051	-0.028	2.8	-30.	12.
13 Jul	1117Z	310.	165.	0.0038	0.0032	-0.030	5.6	-34.	20.
13 Jul	1117Z	234.	179.	0.0028	0.0032	-0.041	5.6	-15.	26.
13 Jul	1359Z	187.	89.	0.0045	0.0022	-0.048	3.0	-34.	11.
13 Jul	1410Z	187.	96.	0.0055	0.0217	-0.057	3.3	-33.	12.
13 Jul	1420Z	197.	113.	0.0036	0.0258	-0.063	1.9	-17.	16.
13 Jul	1429Z	210.	126.	0.0032	0.0207	-0.057	1.1	-15.	18.
13 Jul	1439Z	230.	113.	0.0031	0.0141	-0.043	2.7	-24.	15.
13 Jul	1448Z	234.	113.	0.0032	0.0141	-0.043	2.8	-25.	15.
13 Jul	1458Z	224.	99.	0.0034	0.0170	-0.049	2.2	-28.	13.
13 Jul	158Z	234.	96.	0.0032	0.0118	-0.044	2.7	-26.	12.
13 Jul	1517Z	217.	96.	0.0033	0.0119	-0.042	2.8	-29.	12.
13 Jul	1526Z	200.	122.	0.0033	0.0121	-0.040	2.8	-23.	16.
13 Jul	1536Z	197.	96.	0.0030	0.0119	-0.041	2.2	-26.	13.
13 Jul	1545Z	210.	132.	0.0036	0.0115	-0.040	3.2	-24.	17.
13 Jul	1555Z	234.	139.	0.0044	0.0097	-0.034	4.9	-35.	17.
13 Jul	164Z	227.	139.	0.0045	0.0095	-0.031	5.3	-38.	17.
13 Jul	1613Z	217.	122.	0.0049	0.0081	-0.031	5.7	-47.	13.

REPRODUCED AT GOVERNMENT EXPENSE

Date	Time	Zi	Th	CT <sup>2</sup>	Qo	T*	Δ T	dN/dZ	Δ M
13Jul	1624Z	234.	103.	0.0045	0.0069	-0.032	5.4	-53.	11.
13Jul	1633Z	243.	109.	0.0016	0.0058	-0.024	2.6	-24.	15.
13Jul	1642Z	250.	106.	0.0056	0.0040	-0.021	10.9	-103.	6.
13Jul	1653Z	260.	119.	0.0012	0.0023	-0.011	4.2	-35.	15.
13Jul	17 2Z	290.	152.	0.0022	0.0015	-0.007	13.9	-92.	10.
13Jul	1718Z	293.	113.	0.0017	0.0047	-0.017	4.3	-39.	13.
13Jul	1727Z	296.	136.	0.0009	0.0068	-0.024	1.7	-13.	20.
13Jul	1736Z	296.	96.	0.0010	0.0025	-0.025	1.9	-19.	13.
13Jul	1745Z	310.	149.	0.0013	0.0036	-0.015	4.0	-27.	19.
13Jul	1754Z	323.	79.	0.0021	0.0043	-0.017	5.8	-73.	7.
13Jul	18 5Z	333.	129.	0.0012	0.0045	-0.015	4.0	-31.	16.
13Jul	1814Z	353.	182.	0.0008	0.0042	-0.014	3.0	-17.	26.
13Jul	1825Z	363.	165.	0.0014	0.0033	-0.014	3.5	-30.	21.
13Jul	1836Z	379.	83.	0.0011	0.0024	-0.010	5.7	-69.	7.
14Jul	1053Z	346.	93.	0.0009	0.0012	-0.014	3.3	-36.	11.
14Jul	11 0Z	366.	46.	0.0004	0.0012	-0.014	1.4	-30.	6.
14Jul	11 7Z	346.	129.	0.0005	0.0011	-0.017	1.4	-11.	19.
14Jul	1723Z	320.	106.	0.0018	0.0012	-0.027	3.0	-29.	14.
14Jul	1730Z	320.	149.	0.0009	0.0015	-0.013	3.2	-22.	20.
14Jul	1737Z	326.	89.	0.0011	0.0015	-0.013	4.1	-46.	10.
14Jul	1752Z	343.	106.	0.0011	0.0014	-0.015	3.3	-32.	13.
14Jul	1759Z	343.	109.	0.0018	0.0016	-0.011	8.0	-74.	9.
14Jul	18 8Z	310.	103.	0.0018	0.0016	-0.011	7.5	-73.	9.
14Jul	1815Z	343.	106.	0.0011	0.0024	-0.014	4.0	-38.	13.
14Jul	1822Z	333.	96.	0.0033	0.0017	-0.011	14.0	-146.	1.
14Jul	1829Z	326.	79.	0.0042	0.0017	-0.011	18.4	-233.	-6.
14Jul	1837Z	333.	99.	0.0025	0.0017	-0.011	11.0	-111.	5.
14Jul	1844Z	330.	53.	0.0022	0.0023	-0.013	8.2	-154.	0.
14Jul	1851Z	320.	103.	0.0015	0.0025	-0.015	4.9	-48.	11.
14Jul	1858Z	330.	99.	0.0018	0.0025	-0.015	5.7	-58.	10.
14Jul	19 6Z	320.	99.	0.0024	0.0023	-0.014	5.8	-81.	7.
14Jul	1913Z	333.	106.	0.0018	0.0014	-0.009	9.9	-93.	7.
14Jul	1920Z	323.	89.	0.0013	0.0011	-0.006	10.0	-112.	4.
14Jul	1927Z	330.	83.	0.0038	0.0011	-0.006	30.0	-362.	-17.
14Jul	1942Z	313.	103.	0.0013	0.0015	-0.008	8.2	-80.	8.
14Jul	1949Z	323.	83.	0.0026	0.0015	-0.008	16.2	-195.	-3.
14Jul	1957Z	330.	96.	0.0027	0.0014	-0.008	15.7	-163.	-1.
14Jul	20 5Z	343.	93.	0.0014	0.0011	-0.008	8.2	-89.	6.
15Jul	228Z	313.	86.	0.0040	0.0016	-0.005	35.6	-413.	-22.
15Jul	240Z	310.	126.	0.0055	0.0010	-0.004	68.8	-546.	-49.
15Jul	251Z	320.	142.	0.0033	0.0015	-0.004	34.3	-242.	-12.
15Jul	316Z	313.	79.	0.0027	0.0020	-0.006	21.2	-268.	-9.
15Jul	327Z	310.	109.	0.0049	0.0027	-0.008	26.9	-247.	-10.
15Jul	339Z	303.	126.	0.0025	0.0038	-0.011	10.1	-80.	10.
15Jul	352Z	306.	86.	0.0030	0.0043	-0.013	10.7	-124.	3.
15Jul	4 4Z	303.	76.	0.0033	0.0038	-0.013	11.4	-149.	1.
15Jul	415Z	313.	139.	0.0040	0.0022	-0.008	22.4	-161.	-1.
15Jul	426Z	310.	132.	0.0032	0.0034	-0.011	13.2	-100.	8.
15Jul	439Z	310.	116.	0.0036	0.0032	-0.010	16.5	-142.	2.
15Jul	451Z	326.	106.	0.0037	0.0023	-0.008	23.0	-217.	-6.
15Jul	5 3Z	313.	126.	0.0025	0.0021	-0.008	14.6	-116.	5.
15Jul	514Z	303.	139.	0.0042	0.0028	-0.010	18.5	-133.	3.
15Jul	526Z	303.	129.	0.0029	0.0032	-0.010	12.7	-99.	8.
15Jul	539Z	306.	122.	0.0027	0.0020	-0.007	18.1	-148.	1.
15Jul	550Z	313.	149.	0.0036	0.0017	-0.006	27.4	-184.	-4.
15Jul	6 2Z	313.	113.	0.0014	0.0020	-0.007	9.4	-85.	5.
15Jul	615Z	313.	113.	0.0017	0.0018	-0.006	12.4	-110.	8.
15Jul	1036Z	286.	83.	0.0030	0.0013	-0.004	29.9	-361.	-17.
15Jul	1049Z	290.	79.	0.0030	0.0011	-0.003	39.0	-505.	-28.
15Jul	11 0Z	300.	113.	0.0044	0.0010	-0.003	57.0	-504.	-39.
15Jul	1147Z	300.	126.	0.0048	0.0012	-0.004	52.8	-419.	-33.
15Jul	1159Z	300.	86.	0.0047	0.0018	-0.006	34.8	-405.	-21.
15Jul	1211Z	293.	119.	0.0042	0.0043	-0.014	13.1	-110.	6.
15Jul	1222Z	293.	73.	0.0049	0.0036	-0.012	17.7	-243.	-6.
15Jul	1246Z	283.	126.	0.0015	0.0048	-0.016	4.2	-33.	16.
15Jul	1258Z	253.	76.	0.0033	0.0048	-0.017	7.7	-102.	4.

Date	Time	Zi	Th	CT <sup>2</sup>	Qo	T*	ΔT	dN/dZ	ΔM
15 Jul	1310Z	260.	106.	0.0028	0.0051	-0.014	8.2	-77.	8.
15 Jul	1323Z	273.	113.	0.0027	0.0053	-0.016	7.1	-63.	11.
15 Jul	1334Z	273.	93.	0.0026	0.0066	-0.017	6.5	-70.	8.
15 Jul	1345Z	277.	93.	0.0049	0.0039	-0.011	18.7	-201.	-4.
15 Jul	1359Z	283.	96.	0.0033	0.0050	-0.014	9.8	-102.	5.
15 Jul	1410Z	286.	86.	0.0031	0.0033	-0.011	11.7	-136.	2.
15 Jul	1422Z	283.	96.	0.0032	0.0031	-0.008	16.7	-174.	-2.
15 Jul	1433Z	293.	116.	0.0025	0.0020	-0.005	21.6	-186.	-3.
15 Jul	1444Z	303.	183.	0.0038	0.0014	-0.004	37.8	-455.	-25.
15 Jul	1457Z	306.	129.	0.0029	0.0030	-0.009	14.4	-112.	6.
15 Jul	15 9Z	316.	76.	0.0018	0.0035	-0.010	7.9	-105.	4.
15 Jul	1521Z	320.	73.	0.0025	0.0035	-0.013	8.8	-121.	3.
15 Jul	1532Z	316.	139.	0.0013	0.0039	-0.014	4.3	-31.	18.
15 Jul	1545Z	306.	96.	0.0040	0.0040	-0.016	6.4	-67.	9.
15 Jul	1557Z	296.	89.	0.0023	0.0053	-0.016	10.7	-121.	3.
15 Jul	16 8Z	293.	132.	0.0028	0.0038	-0.014	9.0	-68.	12.
15 Jul	1620Z	263.	106.	0.0022	0.0037	-0.014	6.3	-59.	10.
15 Jul	1737Z	250.	93.	0.0025	0.0060	-0.018	5.5	-59.	9.
15 Jul	1748Z	253.	89.	0.0033	0.0069	-0.023	5.5	-64.	8.
15 Jul	18 0Z	253.	93.	0.0048	0.0065	-0.021	8.9	-96.	6.
15 Jul	1811Z	260.	106.	0.0020	0.0067	-0.022	3.7	-35.	13.
15 Jul	1823Z	277.	116.	0.0015	0.0066	-0.024	2.7	-23.	16.
15 Jul	1836Z	277.	116.	0.0032	0.0056	-0.019	7.1	-62.	11.
15 Jul	1847Z	277.	113.	0.0018	0.0068	-0.021	3.5	-31.	14.
15 Jul	1858Z	263.	73.	0.0044	0.0065	-0.021	8.7	-119.	3.
15 Jul	1912Z	260.	96.	0.0041	0.0052	-0.016	10.5	-110.	5.
15 Jul	2010Z	243.	79.	0.0038	0.0051	-0.015	9.7	-123.	3.
15 Jul	2022Z	257.	89.	0.0063	0.0025	-0.009	28.6	-321.	-15.
15 Jul	2034Z	263.	89.	0.0033	0.0033	-0.011	12.3	-138.	2.
15 Jul	2047Z	263.	96.	0.0055	0.0031	-0.010	23.4	-244.	-8.
15 Jul	2059Z	267.	99.	0.0023	0.0030	-0.010	9.5	-96.	6.
15 Jul	2111Z	270.	99.	0.0032	0.0029	-0.009	15.6	-158.	0.
15 Jul	2122Z	263.	106.	0.0028	0.0020	-0.006	17.8	-168.	-1.
15 Jul	2134Z	270.	109.	0.0042	0.0013	-0.004	45.1	-414.	-28.
15 Jul	2147Z	277.	106.	0.0020	0.0016	-0.005	18.1	-171.	-1.

## LIST OF REFERENCES

Businger, J.A. (1973): *Turbulent transfert in the atmospheric surface layer. Workshop on Micrometeorology*, D.A. Haugen (ed.), American Meteorol. Soc., Boston, pp 1-65.

Davidson, K.L, T.M. Houlihan, C.W. Fairal and G.E. Schacher (1978): *Observation of the temperature structure function parameter,  $CT^2$ , over the ocean.* Boundary-Layer Meteor., 15, pp 507-523.

Dorman, C.E. (1985): *Evidence of Kelvin waves in California's marine layer and related eddy generation.* Monthly weather review, 113, pp.827-839.

Fairal, C.W., R. Markson, G.E. Schacher and K.L. Davidson (1980): *An aircraft study of turbulence dissipation rate and temperature structure function in the unstable atmospheric boundary layer.* Boundary-Layer Meteorol., 19, pp 453-469.

Fleagle, R.G. and J.A. Businger (1980): *An Introduction to Atmospheric Physics.* second editon. Academic Press. N.Y., 432 pp.

Friehe, C.A. (1977): *Estimation of the refractive-index temperature structure parameter over the ocean.* App. Opt., 16, pp. 334-340.

Hitney, H.V., R.A. Paulus, C.P. Hattan, K.D. Anderson and G.E. Linden (1981): *IREPS Revision 2 User's Manual*. Pub. Naval Ocean Systems Center. San Diego, CA., 134 pp.

Johannessen, O.M. and D.A. Horn (1984): *MIZEX 84- Summer experiment preliminary report*. CRREL Special report 84-29.

Meeks, M.L. (1984): *Radar Propagation at Low Altitude*. Artech house, inc. Dedham, MA., 105 pp.

Mohn, M. (1985): *The structure of the atmospheric boundary layer in the marginal ice zone as derived from sodar*. (NPS thesis in preparation).

Monin, A.S. and A.M. Obukhov (1954): *Basic laws of turbulent mixing in the ground layer of the atmosphere*. Akad. Nauk SSSR Geofiz. Inst. Tr., 151, pp. 163-187.

Parry, D.H. and Melvin J. Sanders, Jr. (1972): *The design and operation of an acoustic radar*. IEEE. Trans. on Geosci. Elect., 10, pp. 58-64.

Parry, H.D., Melvin J. Sanders. Jr and H.P. Jensen, (1975): *Operational applications of a pure acoustic sounding system*. J. Appl. Meteor., 14, pp. 67-77.

Wyngaard, J.C., (1973): *On surface layer turbulence*. Chapter 3, Workshop on micrometeorology, D. Haugen, Editor, American Meteorological Society, pp. 101-149.

Wyngaard, J.C., Y. Izumi and S.A. Collins (1971): *Behavior of the refractive index structure parameter near the ground.* J. Opt. Soc. Am., 61, pp 1646-1650.

Wyngaard, J.C. and M.A. Lemone, (1980): *Behavior of the refractive-index structure parameter in the entraining convective boundary layer.* J. Atm. Sci., 37, pp. 1573-1585.

### INITIAL DISTRIBUTION LIST

		No.	Copies
1.	Defense Technical Information Center Cameron Station Alexandria, Virginia 22304-6145.		2
2.	Library, Code 0142 Naval Postgraduate School Monterey, California 93943.		2
3.	Professor C.N.K. Mooers, Chairman Department of Oceanography, code 68Mr Naval Postgraduate School Monterey, California 93943.		1
4.	Professor R.J. Renard, Chairman Department of Meteorology, Code 63Rd Naval Postgraduate School Monterey, California 93943.		1
5.	Professor W.J. Shaw Department of Meteorology, code 63 Naval Postgraduate School Monterey, California 93943.		2
6.	Professor R.W. Garwood Department of Oceanography, code 68 Naval Postgraduate School Monterey, California 93943.		1
7.	Professor K.L. Davidson Department of Meteorology, code 63 Naval Postgraduate School Monterey, California 93943.		1
8.	P. Guest Department of Meteorology, code 63Gs Naval Postgraduate School Monterey, California 93943.		1
9.	Doctor Leonard Johnson Office of Naval Research Arctic Science 800 N. Quincy St., BCT No 1. Arlington, VA 22217-5000.		1
10.	Doctor Paul Twitchell Code Air-330 Naval Air Systems Command. Washington D.C. 20360.		1

11. Docteur J.C. Gascard 1  
Laboratoire d'Océanographie Physique  
Museum d'Histoire Naturelle  
43, rue Cuvier  
75231 Paris cedex 05, France.
12. Docteur A. Weill 1  
Centre de Recherche en Physique de l'Environnement  
CNET  
38-40, rue du Général Leclerc  
92131 Issy-les -Moulineaux, France.
13. Sheryl Fellbaum 1  
Tamar Neta  
Pat Boyle  
Department of Meteorology, code 63Ds  
Naval Postgraduate School  
Monterey, California 93943.
14. Monsieur l'Amiral 3  
Chef d'Etat-Major de la Marine  
2, rue Royale  
75200 Paris Naval, France.
15. Monsieur le Capitaine de Vaisseau 2  
Attaché Naval auprès de l'Ambassade de France  
4101, Reservoir road NW  
Washington D.C. 20007.
16. Monsieur le Capitaine de Vaisseau 2  
Commandant le CEPMAN  
B.P. 38, 83800 Toulon Naval, France.
17. Capitaine de Vaisseau (e.r) Beydon 1  
Météorologie Nationale (Météo/Maritime)  
92106 Boulogne Billancourt Cedex, France.
18. Monsieur le Directeur de l'EPSHOM 1  
13, rue du Chatellier  
B.P. 426  
29275 Brest Cedex, France.
19. Capitaine de Corvette J.F. Soubrier 1  
Etat-Major de la Marine à Lorient  
B.P. 467  
56324 Lorient, France.
20. Lieutenant de Vaisseau E. de Rougé 7  
Cellule Operationelle d'Environnement de la Marine  
2, avenue Rapp  
75007 Paris, France.
21. Météorologie Nationale 1  
SMM / Documentation  
2, avenue Rapp  
75007 Paris, France.

**END**

**FILMED**

**12-85**

**DTIC**